Graduate School ETD Form 9
(Revised 12/07)

PURDUE UNIVERSITY
GRADUATE SCHOOL
Thesis/Dissertation Acceptance

This is to certify that the thesis/dissertation prepared

By Mousumi Mukhopadhyay

Entitled
LANE DEPARTURE AVOIDANCE SYSTEM

For the degree of Master of Science in Electrical and Computer Engineering

Is approved by the final examining committee:

Dr. Sarah Koskie
Chair

Dr. Yaobin Chen

Dr. John Lee

To the best of my knowledge and as understood by the student in the *Research Integrity and Copyright Disclaimer (Graduate School Form 20)*, this thesis/dissertation adheres to the provisions of Purdue University's "Policy on Integrity in Research" and the use of copyrighted material.

Approved by Major Professor(s): Dr. Sarah Koskie

Approved by: Dr. Yaobin Chen 04/20/2011
Head of the Graduate Program Date

Graduate School Form 20
(Revised 9/10)

PURDUE UNIVERSITY
GRADUATE SCHOOL

Research Integrity and Copyright Disclaimer

Title of Thesis/Dissertation:

LANE DEPARTURE AVOIDANCE SYSTEM

For the degree of Master of Science in Electrical and Computer Engineering

I certify that in the preparation of this thesis, I have observed the provisions of *Purdue University Executive Memorandum No. C-22,* September 6, 1991, *Policy on Integrity in Research.**

Further, I certify that this work is free of plagiarism and all materials appearing in this thesis/dissertation have been properly quoted and attributed.

I certify that all copyrighted material incorporated into this thesis/dissertation is in compliance with the United States' copyright law and that I have received written permission from the copyright owners for my use of their work, which is beyond the scope of the law. I agree to indemnify and save harmless Purdue University from any and all claims that may be asserted or that may arise from any copyright violation.

Mousumi Mukhopadhyay

Printed Name and Signature of Candidate

04/21/2011

Date (month/day/year)

*Located at http://www.purdue.edu/policies/pages/teach_res_outreach/c_22.html

LANE DEPARTURE AVOIDANCE SYSTEM

A Thesis

Submitted to the Faculty

of

Purdue University

by

Mousumi Mukhopadhyay

In Partial Fulfillment of the

Requirements for the Degree

of

Master of Science in Electrical and Computer Engineering

May 2011

Purdue University

Indianapolis, Indiana

To My Parents and My Husband Debangshu Sadhukhan.

ACKNOWLEDGMENTS

I would like to acknowledge Dr. Sarah Koskie for providing guidance and being so instrumental throughout the study. I am much indebted for her valuable advice, supervision and devoting her precious time to the thesis.

I would like to thank Dr. Yaobin Chen for his advice and support. I could never have embarked and started working on this thesis without his prior teachings.

I would like to express my appreciation to Dr. Jaehwan Lee for being a part of my advisory committee.

My gratitude also goes to Sherrie Tucker and Valerie Lim Diemer for all their help through the Master's Program.

Also, I thank my family and especially my husband for encouraging me to pursue the degree.

TABLE OF CONTENTS

Page

LIST OF TABLES

LIST OF FIGURES

Figure Page

SYMBOLS

α_f	side slip angle of front tire
α_r	side slip angle of rear tire
β	side slip angle of vehicle
δ_f	steering angle
$\dot{\delta}_f$	steering angle rate
ζ	damping factor
η_t	tire contact length
θ_f	front tire velocity angle
θ_r	rear tire velocity angle
λ	eigenvalues
μ	adhesion
σ_1	driver's lower torque threshold input
σ_2	driver's upper torque threshold input
ψ_L	relative yaw angle
$\dot{\psi}_L$	yaw rate
B_s	steering system damping coefficient
C_G	center of gravity (CG) of the vehicle
F_f	force applied at the front wheel
F_r	force applied at the rear wheel
I_s	inertial moment of steering system
J	vehicle yaw moment of inertia
K	the state feedback gain matrix
K_p	manual steering column coefficient
L	the total width of the lane

P	solution to matrix Riccati equation
Q	state weighting matrix
R	input weighting matrix
R_s	steering gear ratio
T_a	assistance torque
T_d	the torque applied by the driver on the steering wheel
V_f	velocity at the front wheel
V_r	velocity at the rear wheel
$V(x)$	a positive definite function
a	width of the vehicle
a_c	centripetal acceleration
c_{f_0}	front cornering stiffness
c_{r_0}	rear cornering stiffness
d_{ext}	extended width of the center strip which is less than 'L'
l_f	the distance between the CG of the vehicle and the left wheel
l_r	the distance between the CG of the vehicle and the right wheel
l_s	look-ahead distance
m	total mass
r	radius of curvature
t_0	initial state
t_1	final state
v_x	longitudinal velocity at the center
x	the state vector
x^M	bounds for the first LIVIC switching strategy
$(x^M)_{new}$	bounds for the second LIVIC switching strategy
x^N	state variables bounded to normal driving zone
x^{sw}	a set of the states' values obtained from the simulations
y_l	co-ordinate of the front wheel
y_r	co-ordinate of the rear wheel

y_L	lateral offset with respect to the center of the lane at a look-ahead distance l_s
y_L^{CG}	lateral offset at the center of gravity of the vehicle
$2d$	width of the center strip

ABSTRACT

Mukhopadhyay, Mousumi. M.S.E.C.E., Purdue University, May 2011. Lane Departure Avoidance System. Major Professor: Sarah Koskie.

Traffic accidents cause millions of injuries and tens of thousands of fatalities per year worldwide. This thesis briefly reviews different types of active safety systems designed to reduce the number of accidents. Focusing on lane departure, a leading cause of crashes involving fatalities, we examine a lane-keeping system proposed by Minoiu Enache et al. They proposed a switched linear feedback (LMI) controller and provided two switching laws, which limit driver torque and displacement of the front wheels from the center of the lane.

In this thesis, a state feedback (LQR) controller has been designed. Also, a new switching logic has been proposed which is based on driver's torque, lateral offset of the vehicle from the center of the lane and relative yaw angle. The controller activates assistance torque when the driver is deemed inattentive. It is deactivated when the driver regains control. Matlab/Simulink modeling and simulation environment is used to verify the results of the controller. In comparison to the earlier switching strategies, the maximum values of the state variables lie very close to the set of bounds for normal driving zone. Also, analysis of the controllers root locus shows an improvement in the damping factor, implying better system response.

1. INTRODUCTION

To provide a context for this work, we first discuss the need for safety systems that use sensors to make judgements about when the driver needs assistance to maintain safe control of the vehicle. The next section describes approaches that have been developed to address this need. We decided to focus on lane-keeping system and hence conducted a literature review for lane-keeping systems. We identified a particular lane-keeping system that appeared promising.

1.1 Crash Statistics

According to the World Health Organization (WHO), around 1.2 million people are killed and at least 50 million injured due to vehicle-related accidents every year [1]. The National Highway Traffic Safety Administration (NHTSA) estimates that in 2008, 34,017 fatal crashes involving 50,186 drivers and 37,261 fatalities were reported in United States. 5,870 of these deaths occurred in crashes that involved some form of driver distraction, indicating distraction is a leading cause of accidents in the U.S. [2]. Distractions include fatigue, conversation with passengers, cell phone usage and interaction with other electronic devices such as compact disk players and GPS navigation systems. The NHTSA report also points out that the number of fatal crashes caused by distracted drivers increased from 11% in 2005 to 16% in 2008. A study by the American Association of State Highway and Transportation Officials (AASHTO) reports that, 60% of all fatal crashes involve vehicles departing from their respective lanes [3]. Thus, lane departure is one of the leading causes of accidents which are due to distraction. Deviation of the vehicle from the lane is also one of the leading causes of accidents involving rolling and collision with fixed objects [4].

1.2 Safety Systems

Various safety systems have been developed in the automobile industry to curb the number of accidents. They can be broadly classified into either active safety or passive safety systems. Passive safety systems help protect occupants of a car when a collision occurs. These systems include bumpers, crumple zones, air bags, seat belts, etc. Bumpers act like a cushion and thereby reduce damage to the vehicle body and frame, in case of minor impact. Crumple zones absorb the impact by dispersing the energy during collision through physical deformation of the external frame of the vehicle. Air bags help reduce the rate of deceleration of the driver, in case of an accident. For passenger cars, three-point safety belts are 70% effective for rollover accidents, 50% effective for frontal impact and 55% effective for rear impacts [4]. Three-point safety belt is a single continuous belt integrating lap and shoulder belts together [5]. Passive Restraint systems provide protection, in case of an accident. The restraint systems include airbags and seatbelts with pretensioners. Seatbelts with pretensioners pick up the slack and stretch, providing protection and additional space for air bag to inflate [6] [7], [8].

Active safety systems use information acquired from the vehicle and the environment to try to prevent accidents from happening. Preventive measures may include:

- a warning to the driver, or a correction to the vehicle motion, or
- a preconfiguration of a protective system to respond if a crash occurs.

The ultimate goal of an active safety system is to avoid a crash altogether.

1.3 Active Safety Systems in Production and Under Development

Various active safety features have been developed in the last few decades. Figure 1.1 provides a timeline of active safety system development.

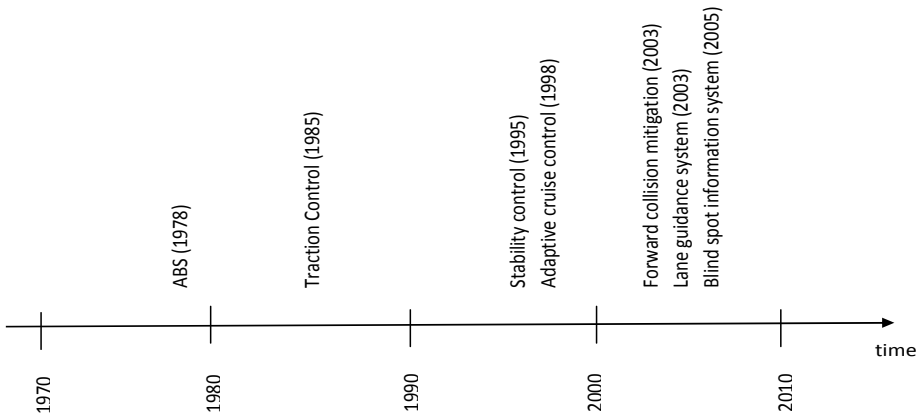

Fig. 1.1. Timeline of active safety system development [9].

1.3.1 ABS (Anti-lock Braking System)

The first ABS system was developed in 1978 [9]. In bad weather conditions, during hard braking, ABS is activated. It prevents locking of wheels during hard braking. By maintaining the longitudinal slip ratio within desired range, ABS tries to maximize the braking forces generated by the tires and thus maintain steering stability. Based on the reading from the wheel mounted sensors, the ABS algorithm holds or releases the brake pressure on the wheel. This is a real time task and execution rate is in milliseconds. The sensors measure the velocity of all four wheels and if, any reading shows a deceleration from its prescribed value, the algorithm reduces the braking pressure.

1.3.2 Traction Control

In 1985, the first Traction Control System was introduced [9]. The traction control system uses the same wheel sensors as the ABS. The algorithm maintains the slip

ratio during acceleration on slippery surfaces. As the slip ratio deviates from the desired range, it limits the power to the driver's wheels and prevents the spinning of the wheels during acceleration. The sensors measure the difference in the rotational speed. Whenever, one of the wheel is spinning faster than the other, engine power is reduced. That is, it will automatically pump the brake to that wheel to reduce its speed and thereby lessen the wheel slip.

1.3.3 Vehicle Stability Control

Vehicle Stability Control was developed in 1995 [9]. The main goal of the control system is to prevent the vehicle from spinning, so that it does not deviate from the desired trajectory. The system measures the yaw rate of the vehicle with respect to its vertical axis. When the road is dry and has a high friction coefficient, the vehicle follows the trajectory that corresponds to the steering wheel angle. If the driver accelerates too fast or coefficient of friction is too small, the vehicle trajectory may deviate from the desired trajectory by failing to maintain the required curve radius. The purpose of a vehicle stability control system is to restore the yaw velocity. Approaches for implementing vehicle stability control may use:

- ABS to apply differential braking,
- Steering control system to modify the steering angle input to provide a correction factor, or
- Stability control system to apply all-wheel drive, wherein there is continuous torque distribution between the left and right wheels using a differential.

1.3.4 ACC (Adaptive Cruise Control)

Adaptive cruise control was developed in 1998 [9]. ACC maintains the current set speed, but also continuously monitors and adjusts the distance to the leading vehicle. This is achieved using forward-looking sensor, usually radar or laser, a digital signal

processor and a robust controller. Whenever the leading vehicle slows down or another object is identified, the system sends a signal to the engine to decelerate. If the leading vehicle increases its speed and ACC detects, the distance to the leading vehicle is safe, ACC slowly accelerates to the set speed. Furthermore, an audible warning is given to the driver, if a higher deceleration is required to avoid a collision. Often, ACC is not considered a safety system by itself, but works along with ABS or Forward Collision Warning (FCW) systems.

1.3.5 Forward Collision Mitigation

Honda has developed Forward Collision Mitigation Systems since 2003 [10]. A Forward Collision Mitigation system integrates all the safety systems discussed above. It uses sensors mounted in front of the bumper to transmit and receive signals which determine the distance and speed of the leading vehicle. Whenever the distance between the vehicles reduces or the leading vehicle slows down, messages and warnings are sent to the mitigation system. The ACC component automatically tries to reduce its speed by reducing the throttle and applying the brakes. A warning is also provided to the driver to take action. If the calibration values surpass the threshold values, ABS provides differential braking. When a collision is inevitable, passive safety features are activated as well. Also, the collision mitigation system decelerates the engine and brakes are applied. The entire communication of the system with the engine and transmission are coordinated through SAE J1939 and other datalink components or tools which have an interface with the Engine Control Module (ECM) [11].

1.3.6 Lane Guidance System

One of the early Lane Guidance Systems was introduced in 2003 [9]. This system can be implemented using:

- Warning system: A system that monitors the position of the vehicle with respect to the center of the lane and provides warning whenever it departs from the lane, or

- Lane-keeping System: A system that automatically takes control of the steering and steers the vehicle back to center of the lane, on detection of the deviation, or

- Combination: A system which is an integration of the first two systems. In addition, it provides audible warnings, steering wheel vibrations etc. It alerts and expects the driver to take control of the vehicle until the vehicle is back to the center of the lane. The automatic steering control is slowly reduced over a period of time.

1.3.7 Blind-spot Warning System

Volvo first introduced a Blind Spot Information System in 2005 [12]. A Blind-spot warning system monitors the adjacent lanes and thereby tries reducing number of lane changing accidents. Various sensors can be used, but commonly radar is used.

1.4 Lane-keeping System

We begin with a brief literary survey. Since a large number of accidents occur due to lane departure, over the last decade, researchers have been working on developing lane-departure avoidance systems. Different aspects of lane-departure have been studied. Researchers have addressed the issue by examining vehicle dynamics, developing lane departure warning systems, devising detection algorithms, integrating sensor technology with the dynamics, etc.

1.4.1 Literature Review

Several studies used the approach of relying on a visual image to detect lane departure. [13] is one such vision-based warning system that alerts the driver of an impending lane departure. The system employs a downward-looking camera to detect the lane markings and warns the driver using a LCD monitor mounted on the dash board. The output of the camera is processed. The time to lane crossing estimation is calculated using the vehicle's lateral position and velocity. Another group has developed a lane detection algorithm for future offset prediction that unites the estimates of the lateral offset with a Kalman filter. The Likelihood of Image Shape (LOIS) algorithm [14] detects the lane markings through a sequence of images and provides a warning. Also, studies have been done on the individual causes of lane departure such as driver drowsiness. The main objective of [15] is to determine a co-relation between driver drowsiness, lane departure and effects of a warning system. A lane departure warning system has been proposed in [16], based on the lateral offset of the vehicle with respect to the center of the lane. In order to detect the lane boundaries, a linear-parabolic model has been used. Extracting the linear part of the model, computations are made to determine the lateral offset without obtaining any information from the camera parameters. Another critical part is predicting the road curvature. The avoidance system in [17] confirms lane departure by acquiring information from the dynamic model and estimation algorithm. For designing an assistance system, studies have been conducted to understand the influence of wind on vehicle dynamics [18]. The thesis proposed an observer model for its estimation.

1.4.2 LIVIC System and Objectives of the Thesis

Minoiu Enache and her colleagues at the Laboratoire sur les Interactions Véhicules-Infrastructure-Conducteurs (LIVIC), a research laboratory for advanced driving assistance systems, addressed the issue of lane departure due to driver inattention in [19]. They proposed a switched linear feedback (LMI) controller and provided two switch-

ing laws for limiting drivers torque and displacement of the front wheels from the center of the lane. They tested their driver assistance system in simulaion and in a vehicle.

The objectives of this thesis are

- to examine the results of the switching strategies outlined by [19] using LQR optimization and
- to propose an improved switching strategy that takes control when the driver is inattentive.

1.5 Motivation and Organization of the Thesis

Based on [19], this thesis aims at developing a lane-keeping system that helps the driver to steer the vehicle back to the center of the lane, when the driver is inattentive. In this thesis, a new switching strategy has been implemented with the help of LQR controller design.

Chapter 2 provides a brief overview of the vehicle dynamics and presents the state-space plant model. Chapter 3 identifies the control objectives, talks about stability analysis and provides a stable control law. Chapter 4 provides a brief overview of the road model followed by the description of the switching strategies developed in [19]. Furthermore, it presents the new switching strategy. Chapter 5 discusses the simulation results for LIVIC 1, LIVIC 2 and the new switching strategy. Chapter 6 concludes the thesis.

2. VEHICLE MODEL WITH STEERING ASSISTANCE

This chapter describes the vehicle model, which was used to test the performance of switching strategy alternatives. As lane-keeping provides lateral control of the vehicle, we need a model of the vehicle lateral dynamics, as well as a model of the steering system. These models are developed in Sections 2.3 and 2.4. Then in Section 2.5 we present the resulting linearized state space equations as described by Minoiu Enache et al. [19].

2.1 Scope of the Model

The environmental model assumes that the effect of road curvature is negligible, so that vehicles can travel at high speeds. The environmental model neglects

- the effect of wind,
- the effect of ground texture, and
- the influence of road bank angle.

For the lateral dynamics, we used the bicycle model, which determines the lateral and yaw dynamics of the wheels and tires, subject to the following assumptions:

- the slip angle at each wheel is zero;
- the vehicle body is rigid between the wheels;
- the vehicle has front wheel steering, i.e. the steering angle for the rear wheels is zero; and
- the vehicle motion is planar.

2.2 The Bicycle Model of Lateral Vehicle Dynamics

The linearized bicycle model is used for its simplicity and ease of implementation. The model represents the two front wheels by a single wheel and, likewise, the two rear wheels by a single wheel. The geometry of the bicycle model is shown in Figure 2.1. The center of gravity of the vehicle is represented by C_G in the figure. The distances between the center of gravity of the vehicle and the left and right wheels are given by l_f and l_r respectively. y_L is the lateral offset with respect to the center of the lane at a distance l_s. l_s is the look ahead distance from the center of the vehicle. The steering angle for the front wheel is represented by δ_f. β is the vehicle side slip angle, and ψ_L is the relative yaw angle which describes the vehicle's orientation. Finally, v_{CG} is the velocity at the center of gravity. In the next section we derive the lateral dynamics of the bicycle model [20].

2.3 Bicycle Model Dynamics

The variables of interest are the side slip β, the yaw angle ψ_L, and the lateral offset y_L from the centerline. First we consider the lateral offset. Equating the velocities at the C_G and the front wheel, the geometry gives us that

$$\dot{y}_L = v_x\beta + l_s\dot{\psi}_L + v_x\psi_L. \tag{2.1}$$

Next we derive the side slip rate. Applying Newton's second law of motion in the lateral direction at the front wheel we have

$$ma_y \;=\; F_f + F_r, \tag{2.2}$$

where m is the total mass of the vehicle, a_y is the lateral acceleration, and F_f and F_r are the lateral tire forces of the front and rear wheel respectively. The lateral acceleration a_y is the sum of $\ddot{y}$ at the vehicle center of gravity and the centripetal acceleration a_c. The centripetal acceleration is given by

$$a_c \;=\; \frac{v_x^2}{R} = v_x\left(\frac{v_x}{R}\right) = v_x\dot{\psi}_L, \tag{2.3}$$

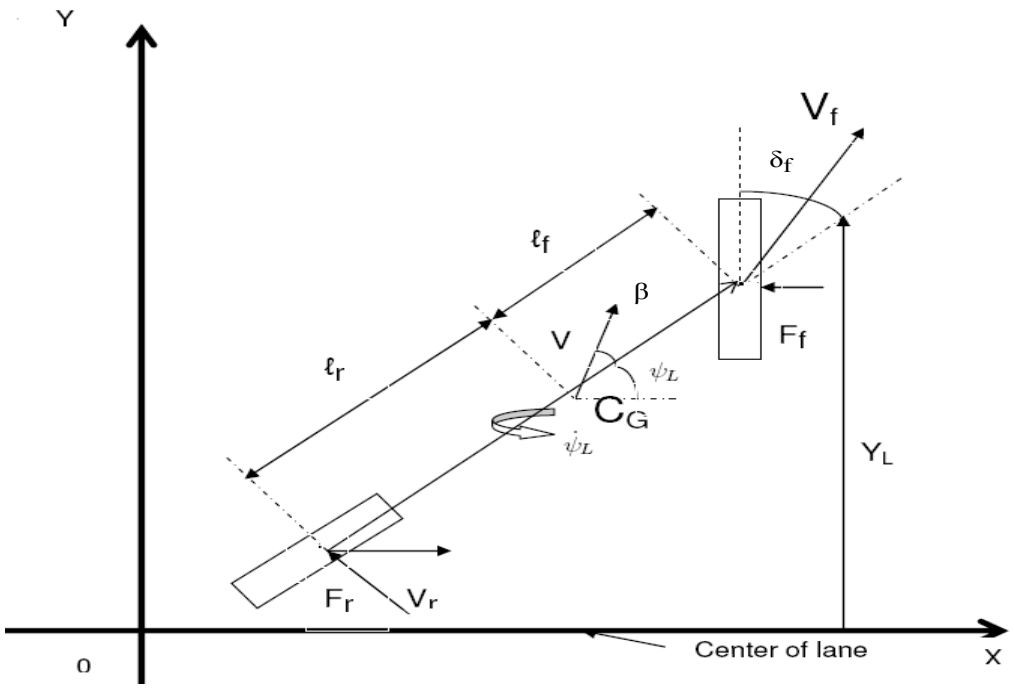

Fig. 2.1. Bicycle model geometry.

where v_x is the longitudinal velocity at the CG of the vehicle and R is the radius of the curvature of the road. Therefore,

$$m(\ddot{y} + v_x\dot{\psi}_L) = F_f + F_r. \tag{2.4}$$

From the geometry, $\cos\beta = v_y/v_x$, where v_y is the lateral velocity at the center of gravity of the vehicle. For small slip angle, $\sin\beta \approx \beta$, so $\dot{\beta} \approx \ddot{y}/v_x$ and (2.2) can be rewritten as

$$m(v_x\dot{\beta} + v_x\dot{\psi}_L) \;\; = \;\; F_f + F_r. \tag{2.5}$$

The lateral tire forces can be expressed in terms of the tire slip angles and cornering stiffness. The slip angle α_f of the tire is the angle between the orientation of tire

and the velocity vector of the wheel. The slip angle β is directly proportional to the lateral tire force when the slip angle is small. As shown in Figure 2.2, the velocity vector makes an angle of θ_f with the longitudinal axis and δ_f is the angle made by the orientation of the tire with the longitudinal axis. Therefore, slip angle of the front wheel α_f is $\delta_f - \theta_f$.

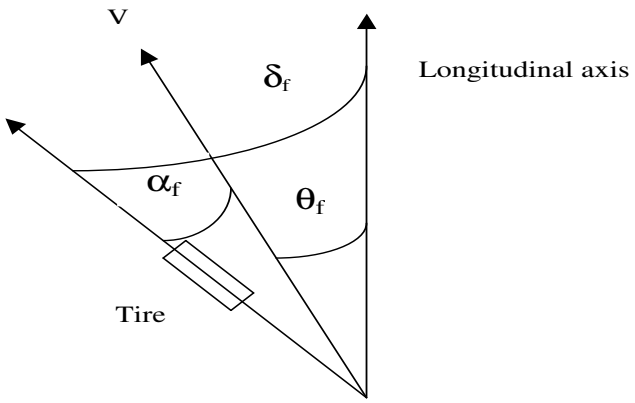

Fig. 2.2. Tire slip angle.

Assuming front wheel steering, the rear wheel slip angle α_r is given by $-\theta_r$, where θ_r is the angle made by the velocity vector at the rear wheel with the longitudinal axis. Hence, the force applied at the front wheel is

$$F_f = 2c_f(\delta_f - \theta_f), \tag{2.6}$$

where c_f is the cornering stiffness. Correspondingly, F_r, i.e. the force applied at the rear wheel, is

$$F_r = 2c_r(-\theta_r). \tag{2.7}$$

Decomposing the velocity vector v into components v_x and v_y along longitudinal and lateral axes respectively, we have

$$\tan(\theta_f) = \frac{v_y + l_f\dot{\psi_L}}{v_x}, \tag{2.8}$$

$$\tan(\theta_r) = \frac{v_y - l_r\dot{\psi_L}}{v_x}. \tag{2.9}$$

Using small angle approximations and noting that $v_y = \dot{y}$, then substituting for F_y and F_x in (2.5) yields

$$mv_x(\dot{\beta} + \dot{\psi_L}) = \frac{2c_f\delta v_x - 2c_f v_y - 2c_f l_f\dot{\psi_L}}{v_x} - \frac{2c_r v_y}{v_x} + \frac{2c_r l_r\dot{\psi_L}}{v_x}, \tag{2.10}$$

which becomes

$$mv_x(\dot{\beta} + \dot{\psi_L}) = -2\beta(c_f + c_r) + \frac{2\dot{\psi_L}(l_r c_r - l_f c_f)}{v_x} + 2c_f\delta_f, \tag{2.11}$$

which can be solved for $\dot{\beta}$ in terms of the states β, $\dot{\psi_L}$ and δ_f to be

$$\dot{\beta} = \frac{-2\beta(c_f + c_r)}{mv_x} + \frac{2\dot{\psi_L}(l_r c_r - l_f c_f)}{mv^2{}_x} - \dot{\psi_L} + \frac{2c_f\delta_f}{mv_x}. \tag{2.12}$$

Finally, the yaw dynamics are obtained by substituting F_f and F_r in the moment balance equation [21].

$$J\ddot{\psi_L} = l_f F_f - l_r F_r \tag{2.13}$$

where J is the vehicle yaw moment of inertia, to obtain

$$\ddot{\psi_L} = \frac{2\beta(l_r c_r - l_f c_f)}{J} + \frac{-2\dot{\psi_L}(l_r^2 c_r + l_f^2 c_f)}{Jv_x} + \frac{2c_f\delta_f l_f}{J}. \tag{2.14}$$

2.4 Steering Dynamics

The steering assistance is provided by a DC motor mounted on the steering column. If a vehicle is traveling straight, then ideally both the velocity angle at the tire (the angle between the velocity vector of the wheel and the longitudinal axis) and the steering angle are both zero, resulting in a zero slip angle. Thus, the slip angles

and the steering angles are assumed to be very small. a is the width of the vehicle, m is the total vehicle mass, Under these assumptions plus the assumption that the velocity vector v is constant (i.e. the velocity vector changes more slowly than the slip angle and yaw angle), we can express the time derivative of the steering angle rate as

$$\ddot{\delta}_f = \frac{T_{S_\beta}}{I_s R_s}(\beta - \delta_f) + \frac{T_{S_{\dot{\psi}_L}}}{I_s R_s} - \frac{B_s}{I_S}\dot{\delta}_f, \tag{2.15}$$

where, R_s is the steering gear ratio, I_s is the inertial moment of steering system, B_s is the steering system's damping coefficient, and T_S is the tire self-aligning torque. The components of the self- aligning torque are given by

$$T_{S_\beta} = \frac{2K_p c_f \eta_t}{R_s}, \tag{2.16}$$

$$T_{S_{\dot{\psi}_L}} = \frac{2K_p c_f \eta_t l_f}{R_s v}, \tag{2.17}$$

where η_t is the tire contact length, K_p is the manual steering column coefficient, and l_f is the distance between the C_G of the vehicle and the left wheel.

2.5 State Space Model

This section provides a linear state-space representation of the vehicle model with steering assistance.

Combining the lateral dynamics and steering dynamics we obtain a sixth order system. The first four states, side slip β, yaw angle ψ_L, yaw rate $\dot{\psi}_L$, and lateral offset y_L correspond to the lateral dynamics. The steering angle δ_f and its derivative comprise the remaining two states. To match the state vector used by Minoiu Enache et al. [19], we order the states as

$$x = \begin{pmatrix} \beta & \dot{\psi}_L & \psi_L & y_L & \delta_f & \dot{\delta}_f \end{pmatrix}^T. \tag{2.18}$$

The state equations are given by

$$\dot{x} = Ax + Bu. \tag{2.19}$$

where,

$$A = \begin{pmatrix} \frac{-2(c_r+c_f)}{mv_x} & -1+\frac{2(l_rc_r-l_fc_f)}{(mv_x^2)} & 0 & 0 & \frac{2c_f}{mv_x} & 0 \\ \frac{2(l_rc_r-l_fc_f)}{J} & \frac{-2(l_r^2c_r+l_f^2c_f)}{Jv_x} & 0 & 0 & \frac{2c_fl_f}{J} & 0 \\ 0 & 1 & 0 & 0 & 0 & 0 \\ v_x & l_s & v_x & 0 & 0 & 0 \\ 0 & 0 & 0 & 0 & 0 & 1 \\ \frac{\left(\frac{2K_pc_f\eta_t}{R_s}\right)}{I_sR_s} & \frac{\left(\frac{2K_pc_fl_f\eta_t}{R_sv_x}\right)}{I_sR_s} & 0 & 0 & \frac{-2K_pc_f\eta_t}{I_sR_s^2} & \frac{-B_s}{I_s} \end{pmatrix}, \tag{2.20}$$

$$B = \begin{pmatrix} 0 \\ 0 \\ 0 \\ 0 \\ 0 \\ \frac{1}{R_sI_s} \end{pmatrix}, \tag{2.21}$$

and

$$c_r = \frac{c_{r_0}}{mu}, \tag{2.22}$$

$$c_f = \frac{c_{f_0}}{mu}, \tag{2.23}$$

where, c_{f_0} is the front cornering stiffness, c_{r_0} is the rear cornering stiffness and μ is the adhesion.

We see that the first three rows of matrix A represent the lateral vehicle dynamics of the bicycle model with two degrees of freedom, which are (2.12), (2.14) and $\dot{\psi}_L = \dot{\psi}_L$. The fourth row refers to the rate of change in lateral offset given by (2.1). The fifth and sixth rows represent the equation for modeling the steering assistance provided by a DC motor mounted on the steering column which was (2.15).

2.6 Chapter Summary

This chapter first derives the bicycle model dynamics, which give the equations for the vehicle lateral and yaw dynamics. It then presents the steering dynamics. The

bicycle model and steering model have been combined together to derive the state space equations as given by Minoiu Enache et al. [19], which provide the vehicle plant model for simulation of the controller.

3. CONTROL LAW DESIGN

In this chapter, we provide the design requirements for the driver assistance system and analyze the stability of the controller. We then provide a brief overview of the LQR optimization technique used in this thesis and apply the technique to obtain the controller gains.

3.1 Design Specifications

Two sets of design criteria are needed: one for the controller and the other for the switching strategy.

Controller specification: The controller must satisfy the following requirements:

1. Stability: Closed loop system must be asymptotically stable to zero steady state. This implies the poles of the closed loop system must lie on the left hand plane. The state variables must be bounded to guarantee safety and comfort.
2. Performance: Damping ratio must lie less than 1.18 and overshoot of the system must be as small as possible.

Switching Strategy: The switching strategy must activate the steering assistance system when the driver is determined to be inattentive and then deactivate the steering assistance system when the driver takes control and the vehicle is back in the normal driving zone. The inputs to the system are T_d, the torque applied by the driver on the steering wheel and T_a, the assistance torque provided by the steering assistance system, during the driver's inattentive time period. For simplicity, the assistance torque selected is

$$T_a = -Kx - T_d \tag{3.1}$$

where, K is the state feedback gain matrix.

The controller design will be described here and the switching strategy will be described in Chapter 5.

3.2 Stability Analysis and Controller Design

The first condition to be met is that system must be asymptotically stable to zero steady state. By definition, the response of the linear system can be always divided into zero-state response and zero-input response.

For the zero-input response, consider an initial state $\mathbf{x_0}$, such that the final state

$$\mathbf{x(t)} = e^{At}\mathbf{x_0}. \tag{3.2}$$

The system is said to be asymptotically stable, if every finite initial state $\mathbf{x_0}$ results in a bounded response that approaches zero as t goes to infinity. A necessary and sufficient condition for asymptotic stability is that all the eigenvalues of A have negative real part.

BIBO stability corresponds to zero state response. A system is said to be Bounded Input Bounded Output (BIBO) stable if every bounded input excites a bounded response. In other words, the zero-state response is BIBO stable if every eigenvalue of A has negative real part.

Analysis of (2.20) indicates that matrix A has two poles at the origin, a pair of complex conjugate poles and two simple poles with negative real part. Thus, the system is only marginally stable.

In order to obtain a stable system, improve the performance of the control strategy, reduce the overshoot and achieve the system objectives, we designed an optimal controller using LQR. LQR design guarantees stability and thus it fulfills the first condition of the design specification.

The linear state-feedback control law u, for the system modeled by $\dot{\mathbf{x}} = A\mathbf{x} + B\mathbf{u}$ is a combination of all the state variables. The state-feedback controller law is of the form

$$\mathbf{u} = -K\mathbf{x}. \tag{3.3}$$

The closed loop system is given by

$$\dot{\mathbf{x}} = (A - BK)\mathbf{x}. \tag{3.4}$$

In order to design a state-feedback controller, the system must be controllable. Hence, we analyzed the controllability matrix for our system analytically. The controllability matrix is given by $[B\ AB\ A^2B\ A^3B\ A^4B\ A^5B]$. This matrix has full rank. Therefore, the final state is reachable. Hence, the system in controllable.

Figure 3.1 illustrates the basic state-feedback controller used to design the closed loop stable controller.

3.3 Linear Quadratic Regulator (LQR)

The cost function for the associated system model using LQR design is:

$$J = \int_0^\infty (x^T Q x + u^T R u) dt, \tag{3.5}$$

where, Q is a non-negative definite state weighting matrix and R is a positive definite input weighting matrix.

High performance is an important criterion for designing industrial control applications. In order to reach steady state, every practical system takes fixed time. During this period it oscillates or increases exponentially. Every system has a tendency to oppose the oscillations. This behavior of the system is called as damping. Damping is measured by the ratio known as damping factor ζ. ζ represents the opposition provided to the oscillations, at the output. By proper selection of the weighing matrices, the time domain performance can be achieved. Q is initially chosen as a 6 x 6 identity matrix and R = 1. The diagonal elements of Q are selected by iteration

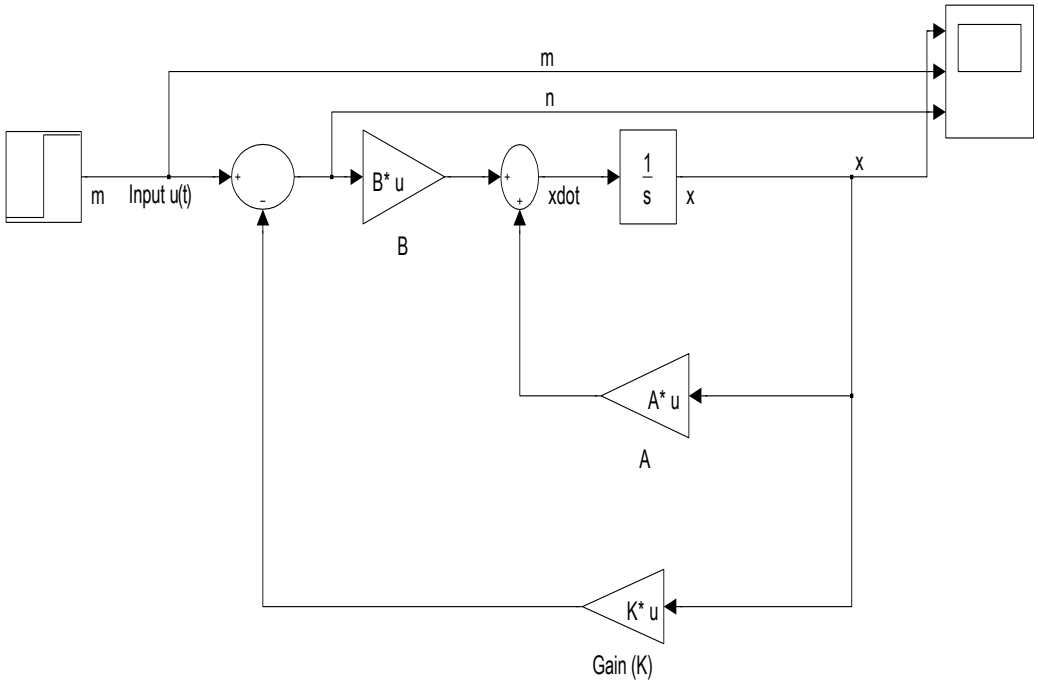

Fig. 3.1. State-feedback controller.

to obtain the feedback matrix. By using root locus, corresponding to the value of the system gain K, i.e., the feedback matrix, a desired damping ratio ζ can be obtained. Hence, the root locus is examined until a damping factor less than 1 and very small overshoot is achieved. It is observed that $0 < \zeta < 1$. This implies that the response is oscillatory, but the amplitude decreases over time. As damping is reduced it is not sufficient to damp the oscillations. Hence, such a system is system is called as under-damped. The dominant pair of roots controls the transient response, i.e. the damping ratio. The real part of complex roots controls the amplitude, while the imaginary part controls the frequency of damped oscillations.

The final matrix Q is of the form

$$Q = \begin{pmatrix} 20 & 0 & 0 & 0 & 0 & 0 \\ 0 & 4 & 0 & 0 & 0 & 0 \\ 0 & 0 & 1 & 0 & 0 & 0 \\ 0 & 0 & 0 & 1000 & 0 & 0 \\ 0 & 0 & 0 & 0 & 20 & 0 \\ 0 & 0 & 0 & 0 & 0 & 100 \end{pmatrix}, \tag{3.6}$$

and R remains unchanged.

The root locus plot of the system, Figure 3.2 shows that the damping factor is less than 1. This implies that the controller is robust to parameter variation. Furthermore, to ensure a robust controller, we considered the gain-margin (GM) and phase margin (PM) of the system, since GM and PM help to maintain closed-loop stability in the presence of errors in the system parameters and neglected dynamics. We used the Matlab robust control toolbox to determine the gain and phase margin at the input of the plant. Using the loopmargin command, we determined that the GM is infinite and the phase margin is 88.8705 deg for the resulting controller.

Using necessary and sufficient condition for unconstrained optimization, we obtain the optimal control law, which is of the form $\mathbf{u}^* = -R^{-1}B^TPx = -Kx$. For a positive definite function $V(x) = x^TPx$, we find an optimal P matrix given by,

$$A^TP + PA + Q - PBR^{-1}B^TP = 0. \tag{3.7}$$

where for a positive definite matrix P, the time derivative evaluated on the trajectories of the closed loop system is negative definite. (3.7) is known as Algebric Riccati Equation (ARE). Thus, the optimal linear controller minimizes the performance index given by (3.5).

Using the controller design, the feedback gain matrix K is of the form,

$$K = \begin{pmatrix} 315.9293 & 44.0141 & 489.7011 & 31.6228 & 682.5164 & 2.4707 \end{pmatrix}. \tag{3.8}$$

The set of closed-loop poles obtained using LQR is given by

$\lambda \varepsilon$ {-297, -11.4, -24.8±1.81i, -1.35±1.69i}.

Hence, the closed-loop system matrix $A = (A - BK)$ has eigenvalues with strictly negative real part.

3.4 Chapter Summary

In this chapter, we have designed a feedback control law to meet the designed specifications outlined in Section 3.1. The resulting controlled system has natural frequency 3.1 rad/s and damping factor 0.808. Thus, from Section 3.2 and 3.3 we can infer that the closed loop system is asymptotically stable. This implies that the system is also BIBO stable. Subsequently, we designed an optimal LQR controller, by proper selection of the weighing matrices, since, the characteristics of the closed-loop response are dictated by the matrices Q and R.

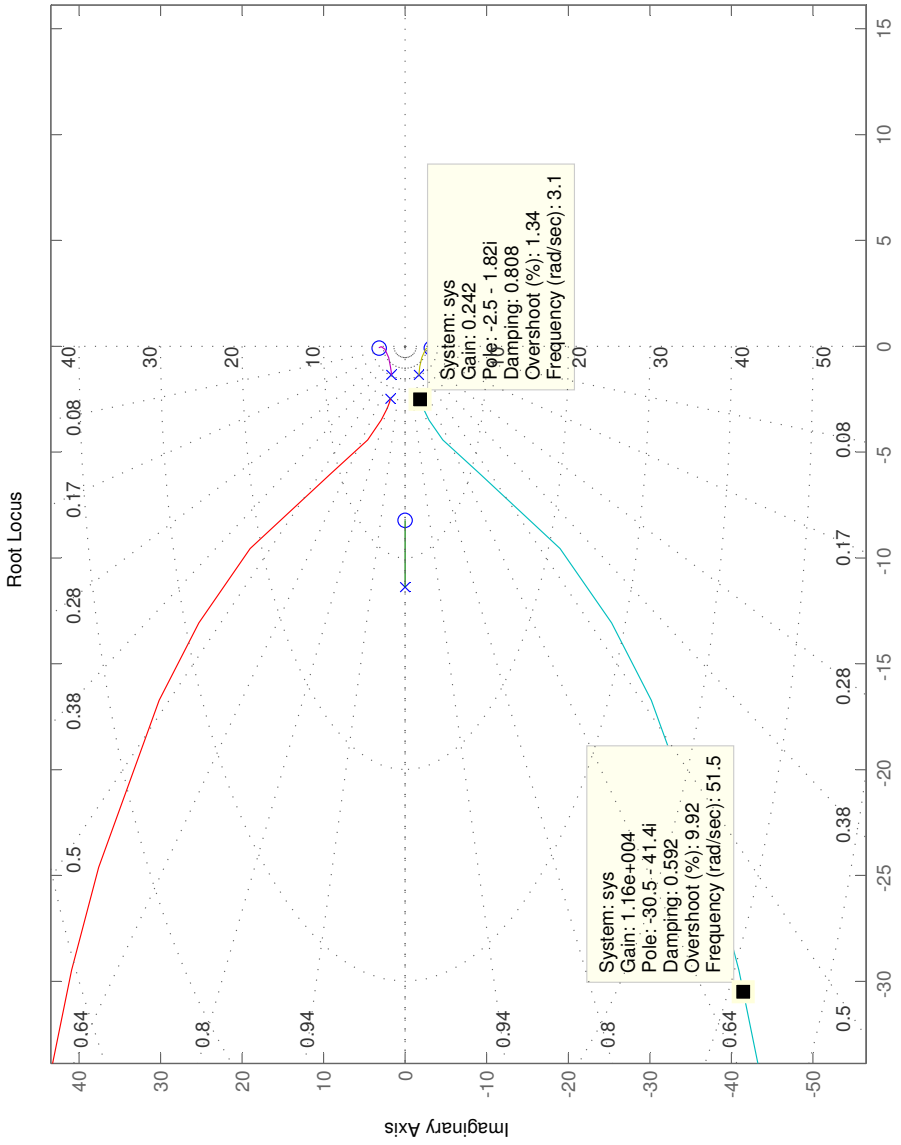

Fig. 3.2. Matlab plot of root locus.

4. SWITCHING STRATEGY

This chapter reviews the road geometry and design specifications in Sections 4.1 through 4.3. Next it discusses the strategies of Minoiu Enache et al. in Section 4.4 and presents a new switching strategy in Section 4.5. The strategies embody the decision mechanism that decides whether the driver is attentive (the vehicle is in the "normal driving zone") or inattentive (the vehicle has deviated from this zone).

4.1 Geometrical Constraints

As described in Section 3.1, when the driver is distracted, the assistance torque is automatically activated and gets deactivated when the driver regains control of the vehicle. When the driver is controlling the vehicle satisfactorily, the coordinates of the front wheels (y_l and y_r) are restricted to the center strip as shown in Figure 4.1.

Fig. 4.1. Normal driving zone of the vehicle.

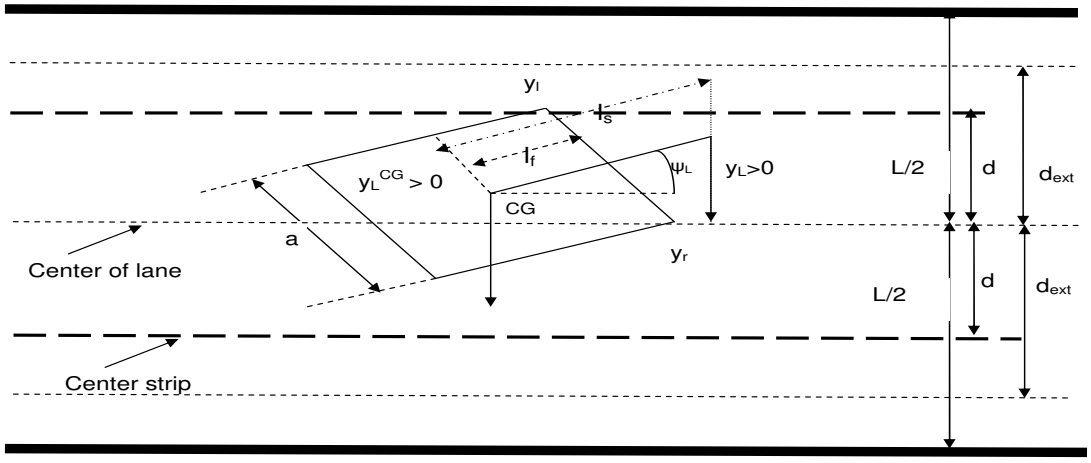

It is assumed that the absolute values of the state variables are bounded within a region given by state vector x^N such that

$$\beta \leq \beta^N, r \leq r^N, \psi_L \leq {\psi_L}^N, y_L \leq {y_L}^N, \delta_f \leq {\delta_f}^N, \dot{\delta}_f \leq \dot{\delta}_f^N. \tag{4.1}$$

where, β^N, r^N, ${\psi_L}^N$, ${y_L}^N$, ${\delta_f}^N$ and $\dot{\delta}_f^N$ are the maximum allowable values for the corresponding state variables. These limits on the state variables correspond to the normal driving zone. There exists, L(F), which is a finite polyhedron in state space defined by Minoiu Enache et al. to define the maximum values of the state variables for normal driving zone, represented by x^N. The set of values for the state variables is obtained in [19] based on their switched LMI controller design.

4.2 Normal Driving Zone

Using the geometric interpretation of the normal driving model, the coordinates of the front wheels are calculated as shown in (4.2) [19]. The relative position of the vehicle with respect to the lane is characterized by the relative yaw angle ψ_L. The lateral offset at the center of the vehicle is y_L^{CG}. The distance of the front axle to the C_G is l_f. a is the vehicle's width. Furthermore, y_L is the lateral offset measured at a look ahead distance l_s using a video camera. l_s is a fixed predetermined look ahead distance from the center of the vehicle. y_l is the coordinate of the front wheel, and y_r is the coordinate of the rear wheel.

$$y_l = y_L^{CG} + l_f \psi_L + a/2, \tag{4.2}$$

$$y_r = y_L^{CG} + l_f \psi_L - a/2. \tag{4.3}$$

Based on our assumptions that the road is straight and the relative yaw angle is small, we can approximate the lateral offset, at the vehicle's center of gravity as $y_L^{CG} \cong y_L - l_s \psi_L$. Hence, we have

$$y_l = y_L + (l_f - l_s)\psi_L + a/2, \tag{4.4}$$

$$y_r = y_L + (l_f - l_s)\psi_L - a/2. \tag{4.5}$$

The condition for the front wheels to be confined to the center strip $2d$ is given by:

$$-2d - a/2 \leq y_L + (l_f - l_s)\psi_L \leq 2d - a/2. \tag{4.6}$$

4.3 Switching Strategy Specifications

The purpose of the switching strategy is to provide assistance torque, when the driver is speculated to be inattentive. The design specifications for implementation of the strategy are based on vehicle lateral trajectory and states' values. The switching strategy is characterized by the requirements that the vehicle should be confined to the center strip, but under no condition should it leave the road. In order to achieve this condition, the vehicle should be restricted within $2d$, i.e. the normal driving zone. The maximum displacement should be less than $d_{ext} = 2.5$ m. d_{ext} is the extended width of the center lane strip which is also constrained to be less than L. Also, the state variables must remain bounded to values experienced under normal driving condition.

4.4 LIVIC Strategies

To address the specifications outlined above, Minoiu Enache et al. proposed two switching strategies, which we will call LIVIC 1 and LIVIC 2.

4.4.1 LIVIC 1 Switching Strategy

The driver's torque T_d has the following thresholds:

- σ_1 which is the lower torque limit and
- σ_2 which is the upper torque limit that is provided as an input to the controller.

σ_1 is set to 2 Nm and σ_2 is set to 6 Nm. The torque limits used in [19] were used here. T_a is the assistance torque which is given by $T_a = Kx - T_d$.

Activation law:

Steering Assistance gets activated when $T_d < \sigma_1$, vehicle is in normal operating zone defined by L(F) and lane crossing has occurred.

Deactivation law:

Steering Assistance gets deactivated when either $\sigma_1 \leq T_d < \sigma_2$ and vehicle is in normal operating zone defined by L(F) or $Td > \sigma_2$, which is indicative of vehicle emergency. Figure 4.2 illustrates this switching logic.

The plot of the switching logic obtained by this implementation is shown in Figure 4.3. At t = 6 s, the driver's torque is less than the lower torque limit σ_1. Hence, the activation criteria are met, summation of driver's torque T_d and assistance torque $T_a + T_d$ is provided at the output of the switching logic. However, as soon as the deactivation criteria is met at t = 19.5 s, the driver's torque, i.e. T_d is provided at the output. The corresponding trajectory of the front wheels is plotted in Figure 4.4.

4.4.2 LIVIC 2 Switching Strategy

In the first strategy, Minoiu Enache et al. missed activating the assistance torque on numerous occasions when vehicle drifted very gradually out of lane and also when vehicle crossed lane very quickly. Additional parameters have been considered for torque assistance activation. The maximum possible displacement of the front wheels is limited to $d_{ext} < 2.5m$. In addition, when the vehicle is close to crossing the lane, the relative yaw angle and lateral offset are simultaneously positive or negative.

Activation Law:

Steering Assistance gets activated when $T_d < \sigma_1$, $d_{ext} \geq 2.5m$, vehicle crossing has occurred and $(\psi_L y_L) = 0$.

Deactivation Law:

The deactivation law remains the same as the first strategy.

Figure 4.5 illustrates this switching logic. The plot of the switching logic is shown in

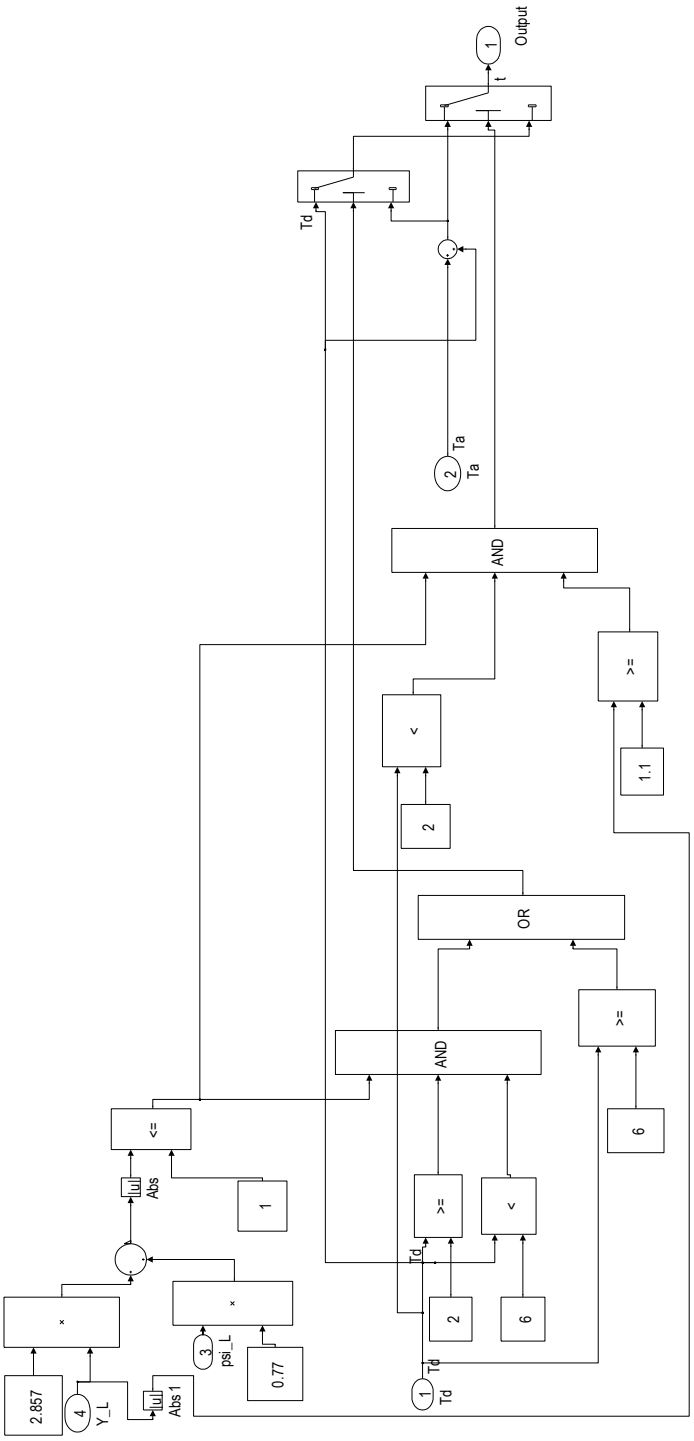

Fig. 4.2. Switching strategy LIVIC 1.

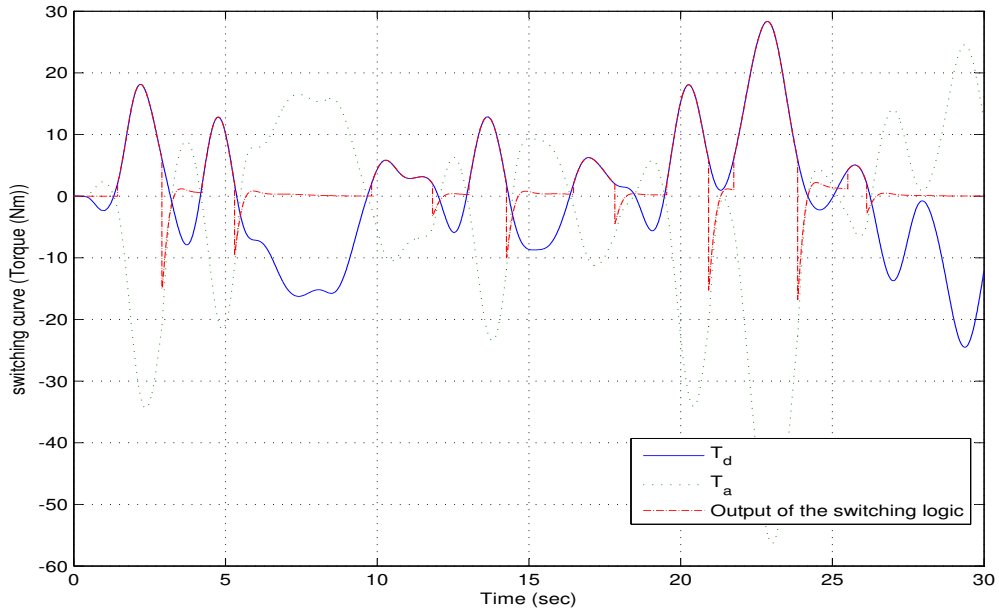

Fig. 4.3. Switching characteristic for LIVIC 1.

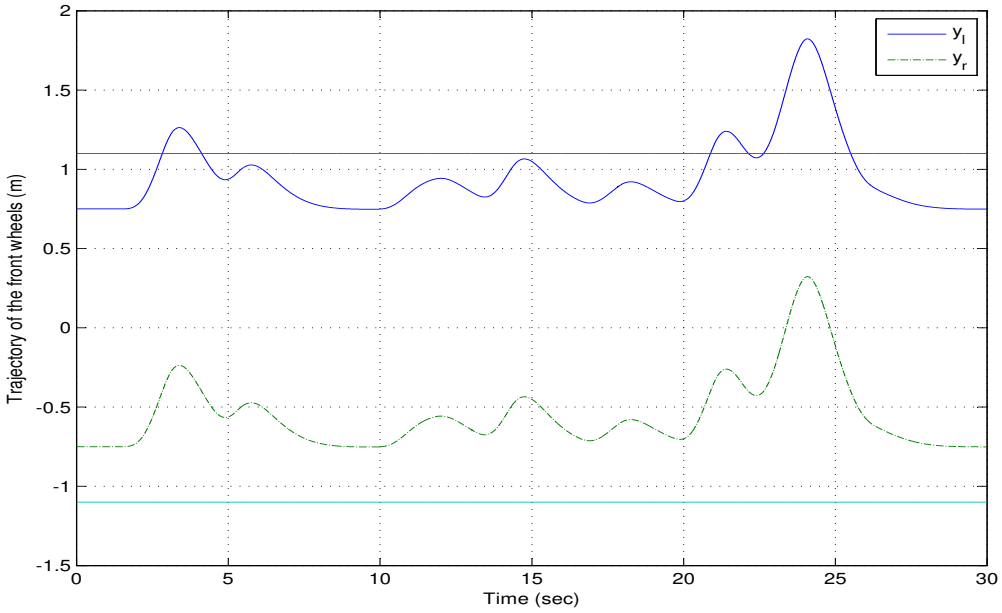

Fig. 4.4. The trajectory of the front wheels.

Figure 4.6. At t = 1 s, the conditions for deactivation law are satisfied. Hence, the output of the switch logic follows the driver's torque. However at t = 3 s, driver's

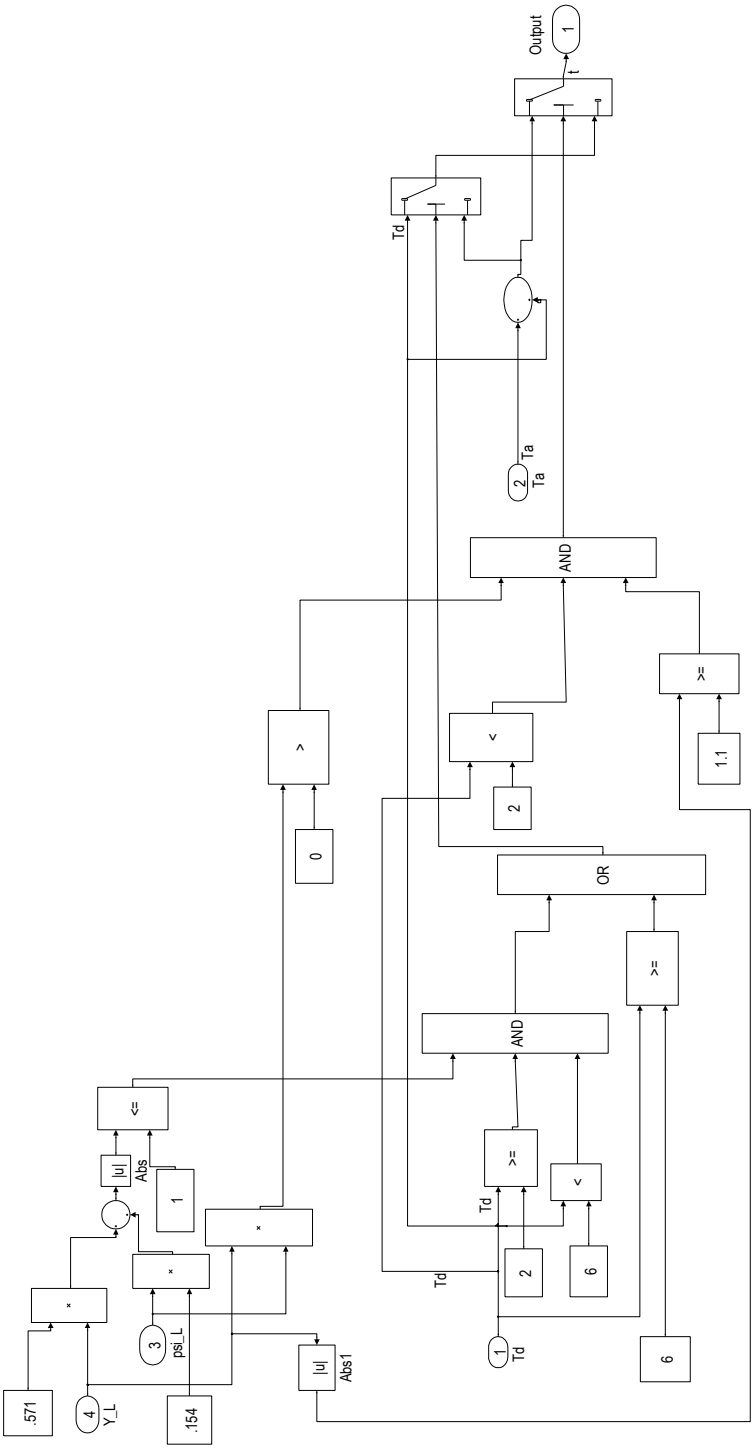

Fig. 4.5. Switching strategy for LIVIC 2.

torque σ_1 is less than lower threshold and the co-ordinate y_l has crossed $d = 1.1m$, which implies lane crossing has occurred. Hence, the output of the switching logic is given by the assistance torque, i.e., $T_a + T_d$. The trajectory of the front wheels is plotted in Figure 4.7.

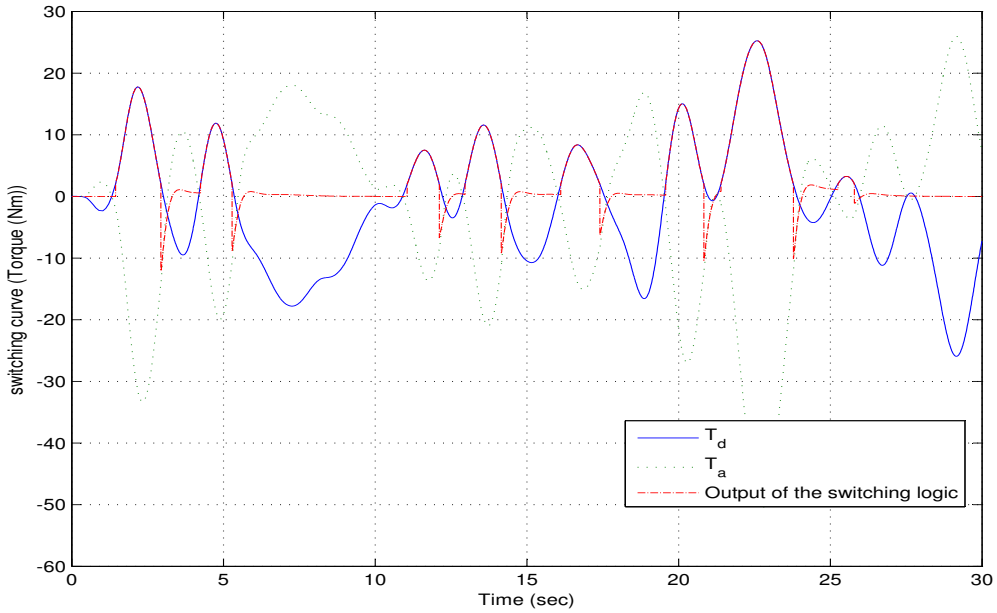

Fig. 4.6. Switching characteristic for LIVIC 2.

4.5 New Switching Logic

In this section, we propose a new switching logic, which satisfies the outlined specifications discussed in Section 4.3.

New deactivation law:

If both the conditions

$$-2d - a/2 \leq y_L + (l_f - l_s)\psi_L \leq 2d - a/2 \tag{4.7}$$

and

$$\sigma_1 \leq T_d \leq \sigma_2 \tag{4.8}$$

are met, then the vehicle follows the desired trajectory. The first condition is to maintain the vehicle within the center strip. This condition also provides the bounds for the state variables. The second condition is to limit the torque input.

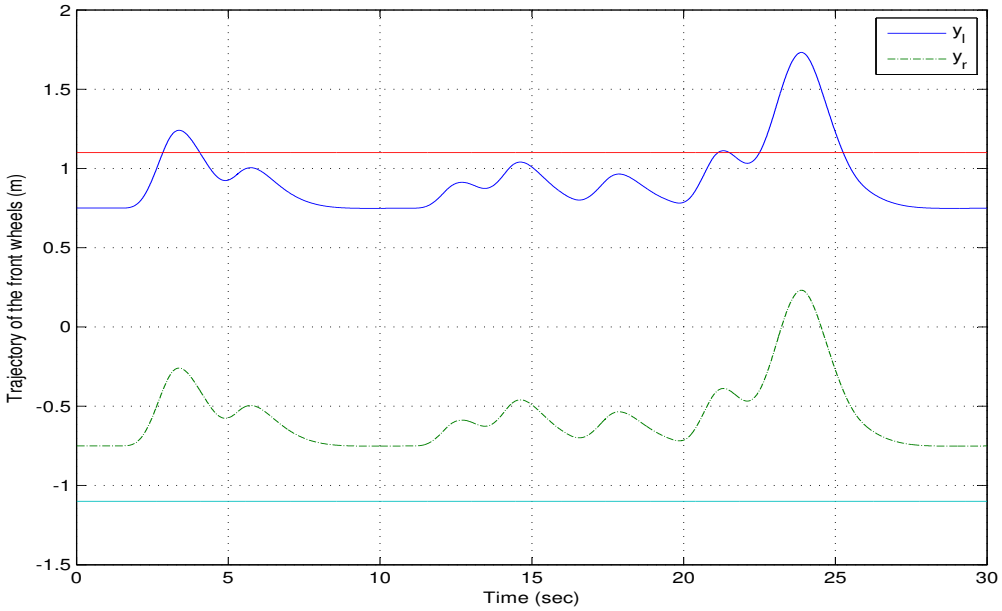

Fig. 4.7. The trajectory of the front wheels for LIVIC 2.

New Activation Law:

Whenever any one of these two conditions is not met, driver is deemed inattentive and the assistance torque $T_a = -Kx - T_d$ is provided. Thus, the switching occurs based on the states y_L, ψ_L and bounds on the driving torque T_d.

Figure 4.8 illustrates this switching logic.

The plot obtained by the implementation of the switching law is shown in Figure 4.9. The output of the switching logic follows the driving torque T_d when the deactivation law is met, at t = 3 s. When the new activation law is met, the assistance torque is provided at t = 4 s. Later, when the value of T_d returns to the specified range given by σ_1 and σ_2 and the vehicle returns to the center of the lane, the assistance torque is deactivated, i.e. at t = 7 s. The trajectory of the front wheels is plotted in Figure 4.10.

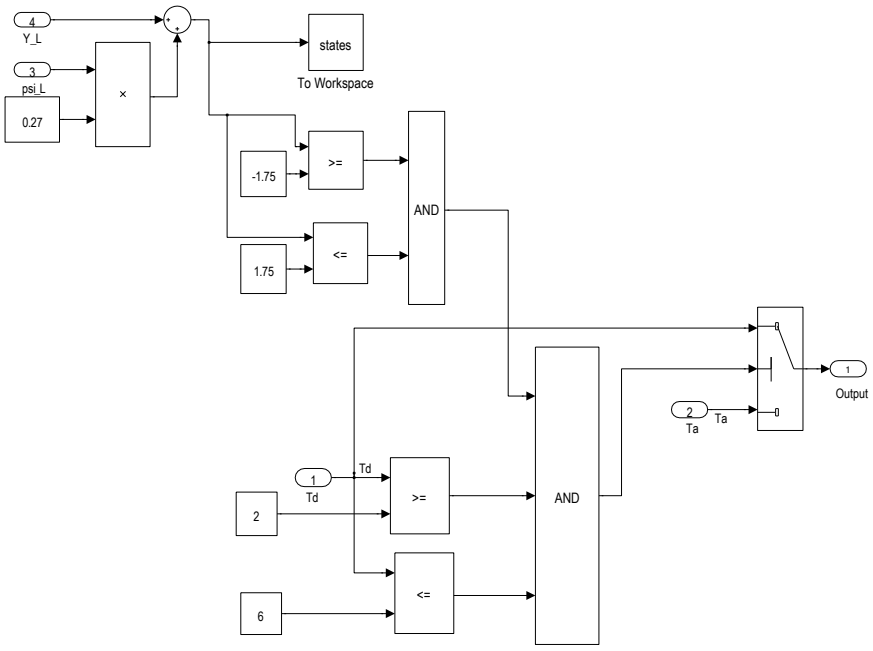

Fig. 4.8. New switching law controller.

4.6 Chapter Summary

This chapter explains the geometric constraints of the lateral control problem and then describes the switching strategies implemented by Minoiu Enache et al. and the new strategy implemented in this thesis. We observe that the driver's torque and width of the center strip plays a critical role in designing the switching strategy.

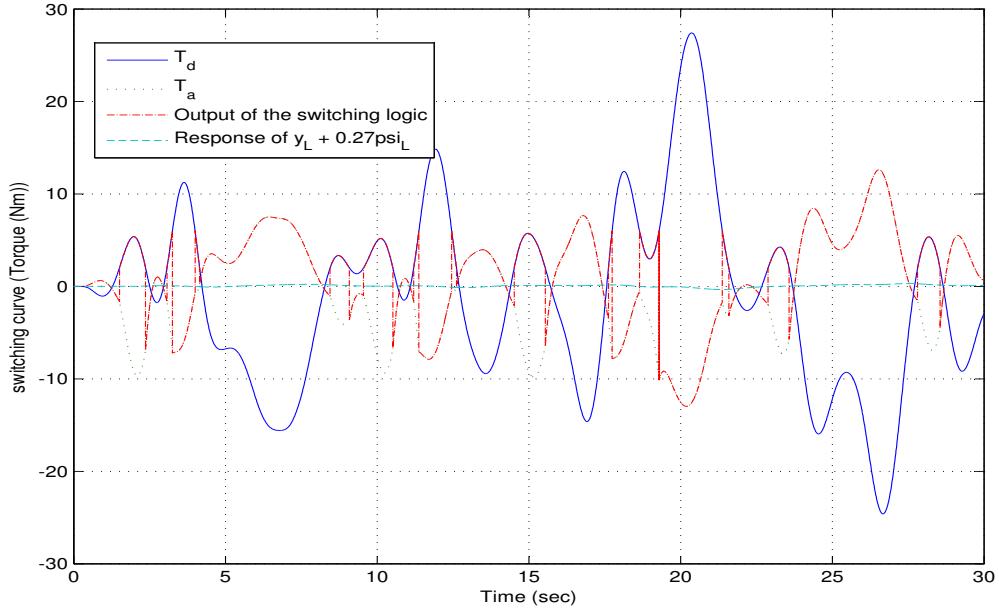

Fig. 4.9. Switching curve for new switching strategy.

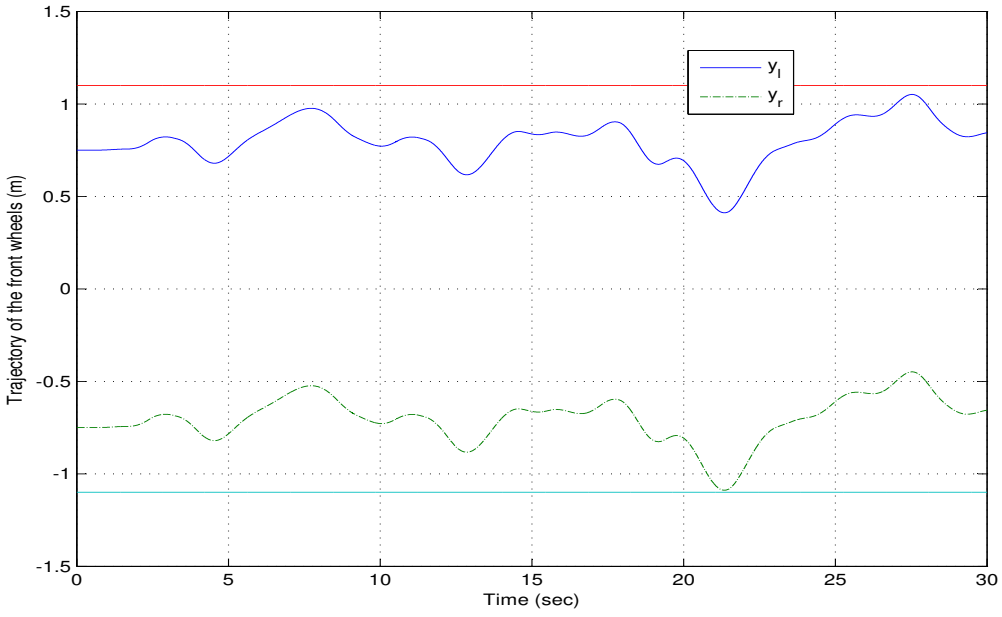

Fig. 4.10. The lateral trajectory of the front wheels.

5. SIMULINK IMPLEMENTATION RESULTS

This chapter presents and compares the simulation results obtained for the switching strategies explained in Chapter 4. The trajectories of the state variables obtained from LIVIC 1, LIVIC 2 and new switching strategy have been compared.

For implementation of the two switching strategies provided by Minoiu Enache et al., a positive state-feedback controller was designed in Matlab. The schematic representation of the state-feedback controller is as shown in Figure 5.1. The feedback matrix K and the torque values given by [19] were used.
$K = (-198.5; -69.3; -355.9; -17.7; -409.9; 5.5)$. Hence, we chose σ_1 and σ_2 to be set at 2 Nm and 6 Nm, respectively.

Our LQR controller designed in Chapter 3 was modeled using Matlab and Simulink for implementing the new switching strategy as discussed in Chapter 4. Figure 5.2 illustrates the block diagram for the designed state-feedback controller.

For all simulations, the driver's torque T_d is represented by a random signal generator, which generates Gaussian distributed random numbers that is filtered using a low pass Bessel filter of the sixth order and cornering frequency 3 rad/s. The Bessel filter preserves the wave shape of the filtered signal in the pass band and hence, preserves the characteristics of the input signal. For simulation of the model, we used

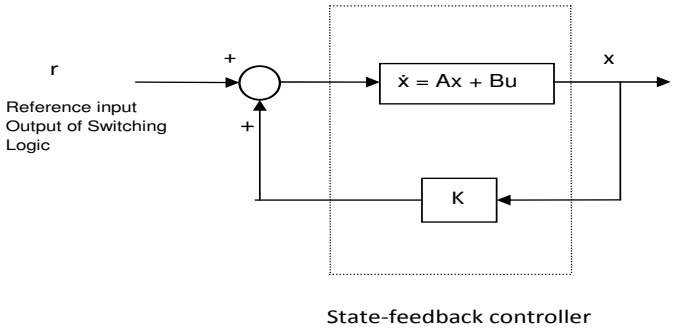

Fig. 5.1. Schematic representation of the controller.

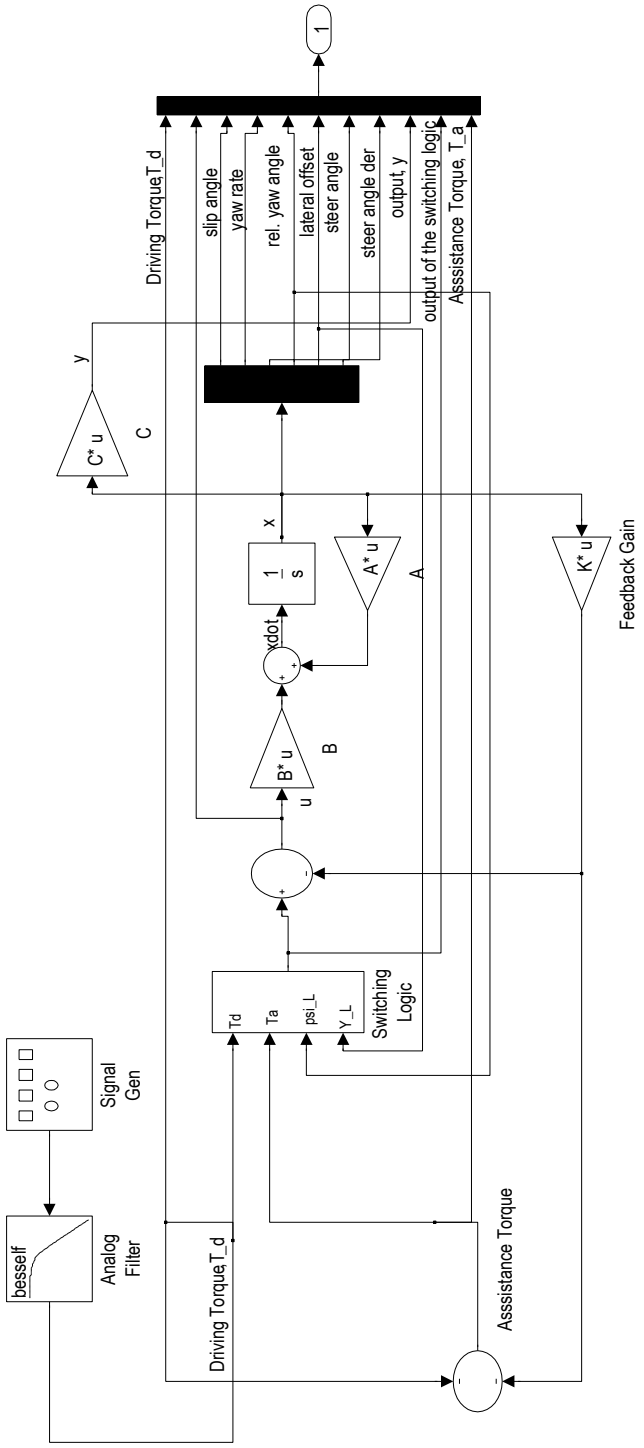

Fig. 5.2. Full state-feedback controller

Matlab R2008a. The solver pane used is Dormand-Prince pair with zero crossing control, which uses variable-step ode45 for the solution. The solver computes the exact value where the signal crosses the x-axis. Figure 5.3 shows the driving torque that is the input to the controller. A driving torque of one Nm corresponds to approximately one third of a meter in displacement.

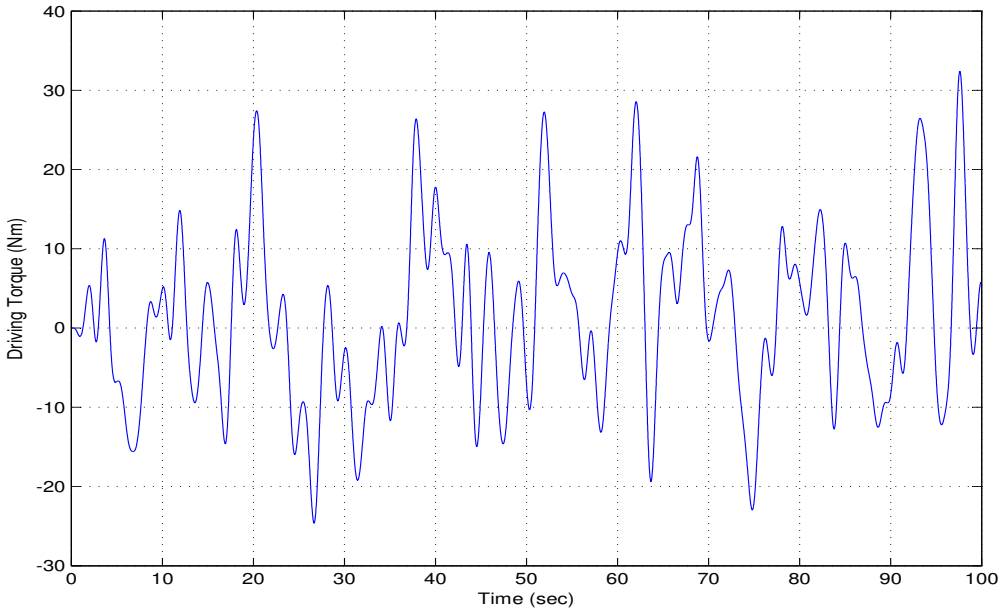

Fig. 5.3. Driver's torque.

We ran the simulation for the new switching strategy obtained in this thesis, using the full negative state-feedback controller model shown in Figure 5.2. In order to provide a good comparison between the new switching strategy and the ones implemented by LIVIC, we set σ_1 to 2 Nm and σ_2 to 6 Nm as well. Also, we ran the simulation for the same amount of time. To obtain the coordinates of the front wheels, we used the following parameters: width of the center strip $2d = 2.2$ m, width of the car $a = 1.5$ m, distance from C_G to the front axle $l_f = 1.22$ m and distance from C_G to the look-ahead distance $l_s = 0.95$ m [19].

5.1 Comparison of Simulation Results

In this section, we compare the plots of the state variables for LIVIC 1, LIVIC 2 and the new switching strategy, for a typical randomly generated driver's torque shown in Figure 5.3.

Figure 5.4 shows the plots of side slip angle for the three switching strategies. We observe that the vehicle's side slip angle for the new switching strategy is maintained very close to zero as desired. Figures 5.5 and 5.6 show the plots of the yaw angle and

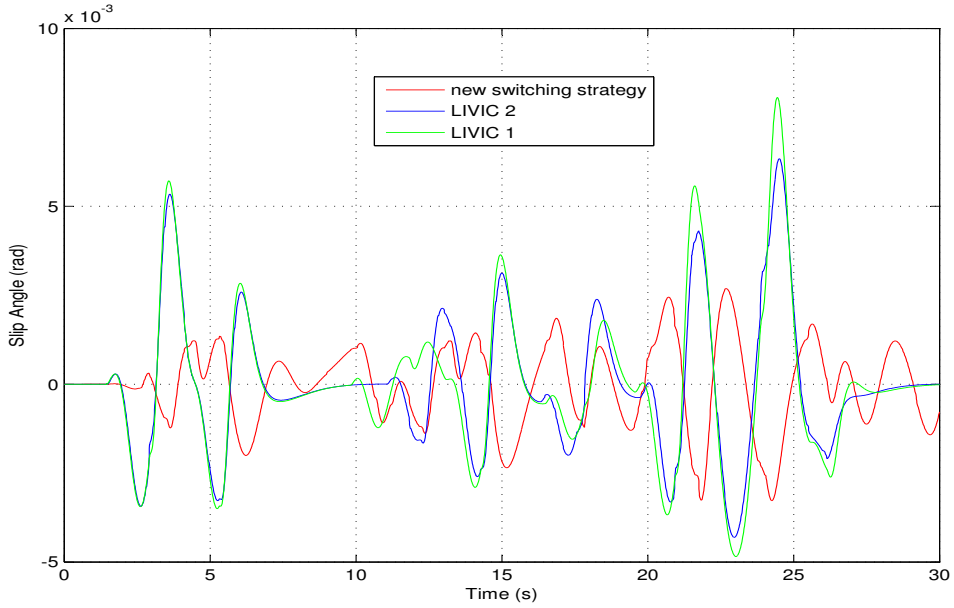

Fig. 5.4. Side slip angle plots for LIVIC 1, LIVIC 2 and new switching strategy.

the yaw rate respectively for the three strategies. Since, we are assuming a straight road, radius of the trajectory of the vehicle changes at a small rate. As a result, we observe that the rate of change in orientation, i.e. yaw rate, is approximately equal to the yaw angle as expected. Figure 5.7 shows the plots of lateral offset of the vehicle for the three strategies. We observe that the lateral offset obtained in the simulation

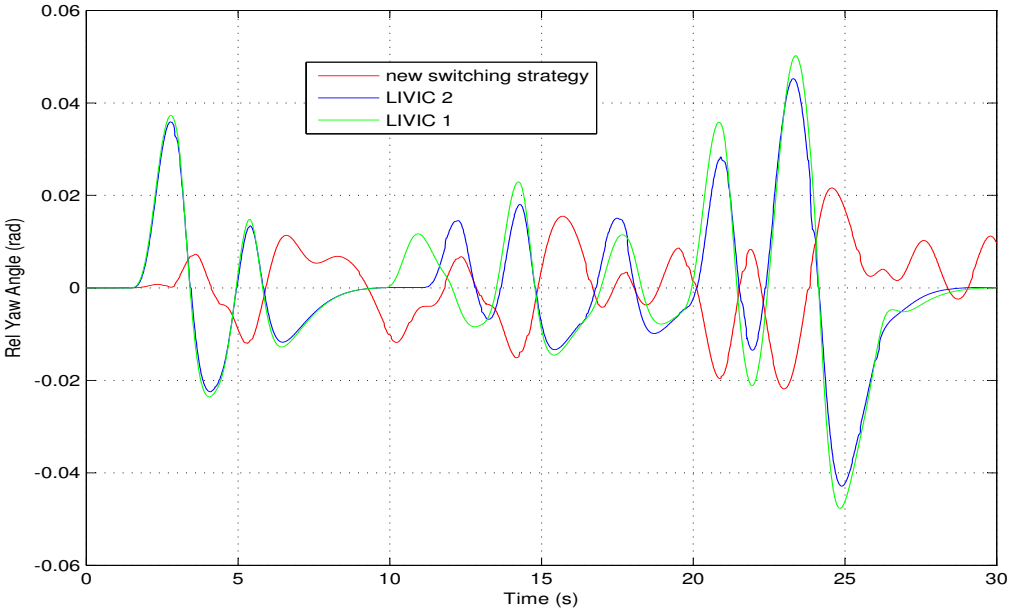

Fig. 5.5. Yaw angle plots for LIVIC 1, LIVIC 2 and new switching strategy.

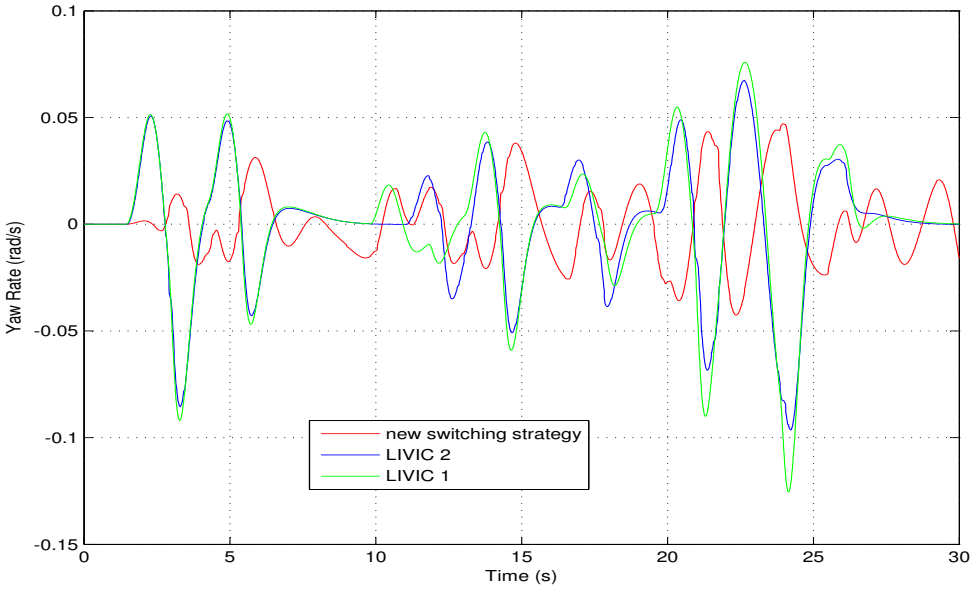

Fig. 5.6. Yaw rate plots for LIVIC 1, LIVIC 2 and new switching strategy.

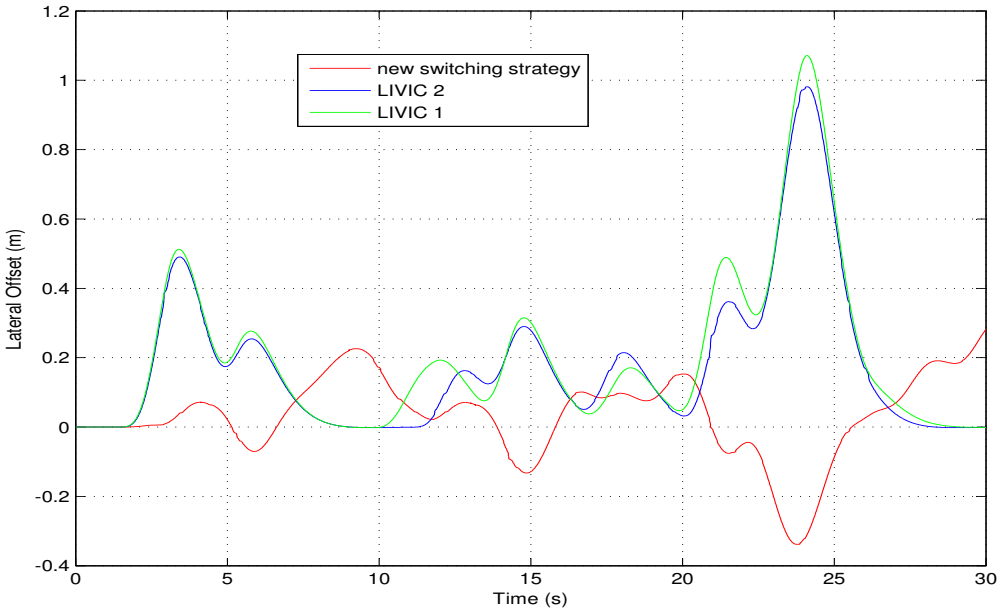

Fig. 5.7. Lateral offset plots for LIVIC 1, LIVIC 2 and new switching strategy.

of the new strategy is bounded closer to zero than that for LIVIC 1 and LIVIC 2. This implies that for the new strategy, the vehicle will be restrained closer to the center line than for the other two strategies. Figures 5.8 and 5.9 show the trajectories of steering angle and rate of change in steering angle respectively for LIVIC 1, LIVIC 2 and new switching strategy. Also, as seen in previous graphs, state variables for the new switching strategy have the least amount of variation.

In order to ensure that the state variables are bounded, we ran the simulations for each switching strategy for durations of 30 s, 60 s and 100 s respectively. Table 5.1 records the maximum values of state variables obtained during the simulations of length 30 s, 60 s and 100 s for LIVIC 1. Similarly, Table 5.2 records the maximum values of state variables obtained during the simulations of length 30 s, 60 s and 100 s for LIVIC 2. Table 5.3 records the maximum values of state variables obtained during

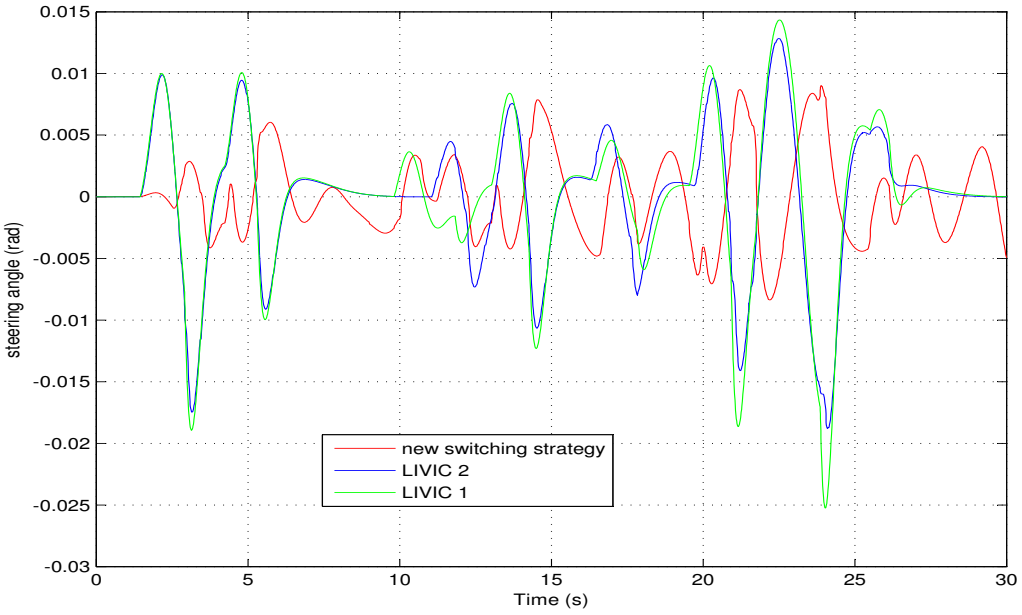

Fig. 5.8. Steering angle plots for LIVIC 1, LIVIC 2 and new switching strategy.

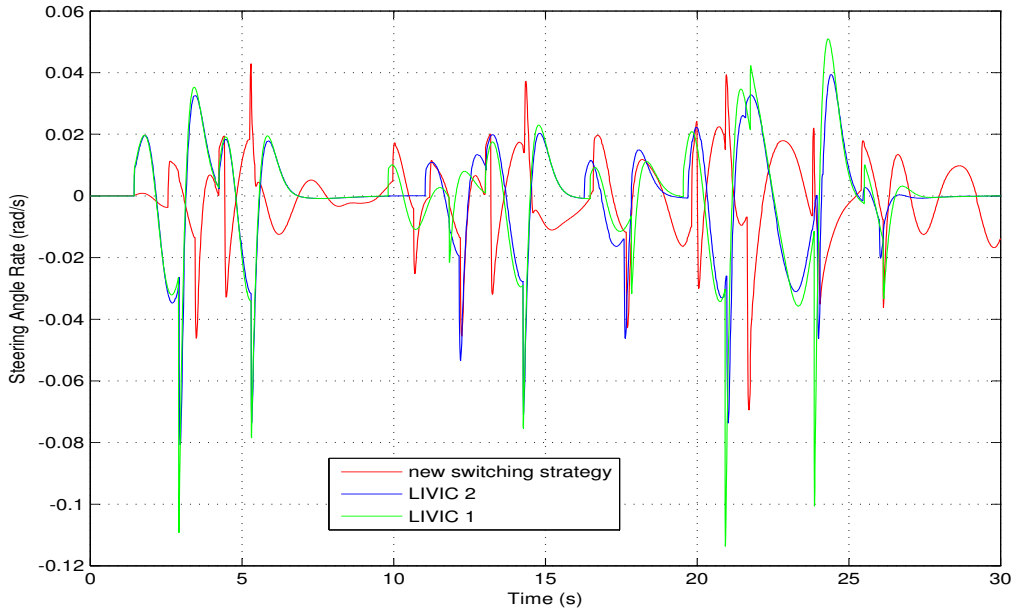

Fig. 5.9. Steering angle rate plots for LIVIC 1, LIVIC 2 and new switching strategy.

Table 5.1
Comparison of maximum values of the state variables for LIVIC 1, at varying simulation time.

	Variable	$30s$	$60s$	$100s$	Units
Side Slip Angle	β_r	0.008	0.008	0.008	rad
Yaw Rate	$\dot{\psi_L}$	0.1255	0.1255	0.145	rad/s
Relative Yaw Angle	ψ_L	0.054	0.058	0.058	rad
Lateral Offset	y_L	1.1	1.2	1.2	m
Steering Angle	δ_f	0.025	0.025	0.028	rad
Steering Angle Rate	$\dot{\delta}_f$	0.1137	0.1137	0.135	rad/s

Table 5.2
Comparison of bounds on state variables at simulation time 30, 60 and 100 s for LIVIC 2.

	Variable	$30s$	$60s$	$100s$	Units
Side Slip Angle	β_r	0.0063	0.0063	0.0072	rad
Yaw Rate	$\dot{\psi_L}$	0.0964	0.0964	0.113	rad/s
Relative Yaw Angle	ψ_L	0.045	0.06	0.061	rad
Lateral Offset	y_L	0.98	0.98	0.98	m
Steering Angle	δ_f	0.0188	0.0188	0.019	rad
Steering Angle Rate	$\dot{\delta}_f$	0.08	0.0739	0.08	rad/s

the simulations of length 30 s, 60 s and 100 s for the new switching Strategy. The results suggest that the state variables for all the three strategies are bounded. In order to compare the results of the new strategy with those implemented by Minoiu Enache et al., Table 5.4 was created. It shows the maximum values of the state

Table 5.3
Comparison of bounds on state variables at simulation time 30, 60 and 100 s for the new switching strategy.

	Variable	$30s$	$60s$	$100s$	Units
Side Slip Angle	β_r	0.0033	0.0033	0.0043	rad
Yaw Rate	$\dot{\psi}_L$	0.0426	0.0426	0.05	rad/s
Relative Yaw Angle	ψ_L	0.0219	0.0275	0.034	rad
Lateral Offset	y_L	0.34	0.34	0.37	m
Steering Angle	δ_f	0.00085	0.00089	0.009	rad
Steering Angle Rate	$\dot{\delta}_f$	0.0695	0.085	0.085	rad/s

variables for the three strategies when simulation was run for 100 s.
The variable

$$x^N = \begin{pmatrix} \beta^N & \dot{\psi}_L^N & \psi_L^N & y_L^N & \delta_f^N & \dot{\delta}_f^N \end{pmatrix}^T \tag{5.1}$$

is the bound on the normal driving zone as given by (4.1). x^M corresponds to the bounds provided by LIVIC 1. $(x^M)_{new}$ shows the observed upper limit on the magnitudes of the state variables for LIVIC 2. x^{sw} shows the observed bounds of magnitudes of the state variables obtained by implementation of the new switching strategy.

5.2 Impact on Vehicle Drivability

From the comparison of the simulation results, we observe that the new strategy restricts the slip angle closest to zero. This implies that the vehicle will have better cornering ability and steering response. Also, the smaller variation in yaw angle and yaw rate for the new strategy will help a driver to maneuver the vehicle with increased confidence. The lateral offset, which is bounded closer to zero, enables better lane-keeping capability. Finally a lower variation in the steering angle and steering angle rate will enable driver to maneuver the vehicle with comparatively less effort.

Table 5.4
Comparison of bounds on state variables for normal driving zone and different switching strategies.

	Variable	x^N	x^M	$(x^M)_{new}$	x^{sw}	Units
Side Slip Angle	β_r	0.0104	0.008	0.0072	0.0043	rad
Yaw Rate	$\dot{\psi}_L$	0.1047	0.145	0.113	0.05	rad/s
Relative Yaw Angle	ψ_L	0.0349	0.0589	0.061	0.034	rad
Lateral Offset	y_L	0.8	1.2	0.98	0.37	m
Steering Angle	δ_f	0.0261	0.028	0.019	0.009	rad
Steering Angle Rate	$\dot{\delta}_f$	0.2094	0.135	0.08	0.085	rad/s

However, the new strategy may have a few disadvantages when incorporated in a real world vehicle. It will control the vehicle more rigidly than LIVIC 1 and LIVIC 2 within the center strip and will provide more resistance against an attempted lane change. The assistance torque is activated for a longer duration, which implies that the hydraulics will be activated longer, eventually leading to a slight decrease in fuel efficiency.

6. CONCLUSION AND FUTURE WORK

In this thesis, we have implemented a lane keeping system. The lane keeping system is comprised of two parts namely the switching strategy that activates and deactivates the assistance torque and a negative feedback LQR controller. Analysis of the designed closed loop system shows that, the real part of the poles lie strictly in the left hand plane. Hence, the system is asymptotically stable. Also, using the LQR optimization method, good time domain performance has been achieved. The system is under-damped, having damping ratio less than one and the overshoot of the system is reduced, which ensures a fast system response. Simulations have been done using the new switching strategy and LQR controller. The simulation results indicate that the state variables are not only bounded, but are also within the normal driving zone. Also, the strategies mentioned in [19] are simulated and the results have been compared with this new strategy. Comparison shows that the bounds of the state variables are lower for the new strategy which should ensure better driver comfort and lane keeping capability. The model is more simplistic than LIVIC 1 and LIVIC 2. Hence, the resulting code will be computationally less intensive. The trajectory of the front wheels obtained for the new controller, clearly shows that it controls more efficiently and maintains the trajectory of the vehicle within absolute value of d from the centerline.

The next steps to this thesis would be to incorporate this controller strategy in a real world vehicle and confirm the simulation results.
However, certain assumptions are made in the bicycle model.

- The equations for lateral vehicle dynamics are non-linear. These equations are linearized by assuming velocity vector is changing more slowly than the state variable slip angle and yaw angle.

- If a vehicle is traveling straight, then the velocity angle at the tire and the steering angle are both zero. For calculations, slip angles and steering angles are assumed to be very small.

Some of these assumptions may be violated in real world driving, in which case the dynamic modeling may need to be revisited.

Also, a good suite of sensors will have to be selected to measure the state variables. Sensors selected should have minimum noise, sensor drift, sensitivity error and hysteresis. A DC motor will need to be selected to provide the assistance torque on the steering column. Also the steering assistance system could be augmented to include audible or haptic warnings to alert the driver that the vehicle is not operating within the acceptable zone.

Emergency lane changing was addressed in LIVIC 1 and LIVIC 2. One of the deactivation criteria for assistance torque was that the driver's torque had to be greater than a threshold, which indicated intentional lane departure. While this has not been addressed in the strategy proposed in this thesis, for the real world implementation the turn signal indicator can be used as an input to the control strategy to deactivate the assistance torque and enable intentional lane changing.

To improve the realism of the dynamic model, the effects of road curvature may need to be considered. On a circular road of radius r, the lateral tire force is mv^2/r, where v^2/r is the centripetal acceleration. Also the road gradient and road bank angle may need to be accounted for in the dynamic model.

LIST OF REFERENCES

LIST OF REFERENCES

[1] M. Peden, R. Scurfield, D. Sleet, D. Mohan, Adnan A. Hyder, E. Jarawan, and C. Mathers, eds., *World report on road traffic injury prevention*. Geneva: World Health Organization, 2004.

[2] D. Ascone, T. Lindsey, and C. Varghese, "An examination of driver distraction as recorded in NHTSA databases," *NHTSA Traffic Safety Facts: Research Note*, September 2009.

[3] American Association of State Highway and Transportation Officials, *Driving Down Lane-Departure Crashes: A National Priority*. Washington, DC: American Association of State Highway and Transportation Officials (AASHTO), 2008.

[4] J. N. Kanianthra, "Accelerating innovative safety technologies into the fleet." AORC Panel Discussion, National Highway Traffic Safety Administration, March 2006.

[5] National Highway Traffic Safety Administration, "49 CFR Part 571," Tech. Rep. Docket No. NHTSA 2010 0112 RIN 2127 AK56, Department of transportation, Washington, DC, 2004.

[6] Skoda, "Sustainable development," 2008. Available at, http://new.skoda-auto.com/Documents/EnvironmentTechDev/Safety_07_2008.pdf. Last accessed April 2011.

[7] R. N. Rob Cirincione, *Innovation and Stagnation In Automotive Safety and Fuel Efficiency*. Washington, DC: Center for the Study of Responsive Law, February 2006.

[8] J. Zhou, *Active Safety Measures for Vehicles Involved in Light Vehicle-to-Vehicle Impacts*. PhD thesis, Department of Mechanical Engineering, The University of Michigan, 2009.

[9] A. Eidehall, *Tracking and threat assessment for automotive collision avoidance*. PhD thesis, Department of Electrical Engineering, Linköping University, Linköping, Sweden, 2007.

[10] CSR Department, Administration & Legal Division, "Safety for everyone in our mobile society," in *Honda CSR Report 2006*, pp. 23–32, Honda Motor Co., Ltd., 2006. Available at, http://world.honda.com/CSR/pdf. Last accessed January 2011.

[11] SAE International, Warrensville, PA, *Recommended Practice for a Serial Control and Communications Vehicle Network. SAE J1939*, October 2007.

[12] J. Lefley, S. Atkins, J. Rawlings, and A. Baker, "UK overview, prices and specifications 2005 model year s60, v70 and xc70." Volvo S60 Press Information release, May 2004.

[13] M. Chen, T. Jochem, and D. Pomerleau, "Aurora: A vision-based roadway departure warning system," in *Proceedings of the IEEE Conference on Intelligent Robots and Systems*, vol. 1, pp. 243–248, 1995.

[14] C. Kreucher, S. Lakshmanan, and K. Kluge, "A driver warning system based on the LOIS lane detection algorithm," in *Proceedings of the IEEE International Conference on Intelligent Vehicles*, pp. 17–22, 1998.

[15] M. Rimini-Doering, T. Altmueller, U. Ladstaetter, and M. Rossmeier, "Effects of lane departure warning on drowsy drivers' performance and state in a simulator," in *Proceedings of the 3rd International Driving Symposium on Human Factors in Driver Assessment, Training and Vehicle Design*, (Rockport, Maine), pp. 88–95, 2005.

[16] C. R. Jung and C. R. Kelber, "A lane departure warning system using lateral offset with uncalibrated camera," in *Proceedings of the 8th International IEEE Conference on Intelligent Transportation Systems*, (Vienna), pp. 348–353, September 2005.

[17] T. B. Schön, A. Eidehall, and F. Gustafsson, "Lane departure detection for improved road geometry estimation," in *Proceedings of the IEEE Intelligent Vehicles Symposium*, pp. 546–551, 2006.

[18] S. Glaser, S. Mammar, and J. Dakhlallah, "Lateral wind force and torque estimation for a driving assistance," in *Proceedings of the 17th World Congress, The International Federation of Automatic Control*, (Seoul, Korea), pp. 5688–5693, 2008.

[19] N. Minoiu Enache, M. Netto, S. Mammar, and B. Lusetti, "Driver steering assistance for lane departure avoidance," *Control Engineering Practice*, vol. 17, pp. 642–651, 2009.

[20] R. Rajamani, *Vehicle Dynamics and Control*. Springer, 2006.

[21] U. Kiencke and L. Nielsen, *Automotive Control Systems, For Engine, Driveline, and Vehicle*. Springer, 2005.

APPENDICES

Appendix A: Block Diagram of Simulation Model

In this chapter, the Matlab block diagram used for implementation of LIVIC 1 and LIVIC 2 are represented in Figure A.1. Figure A.2 represents the negative state-feedback controller used for the implementation of the new switching strategy.

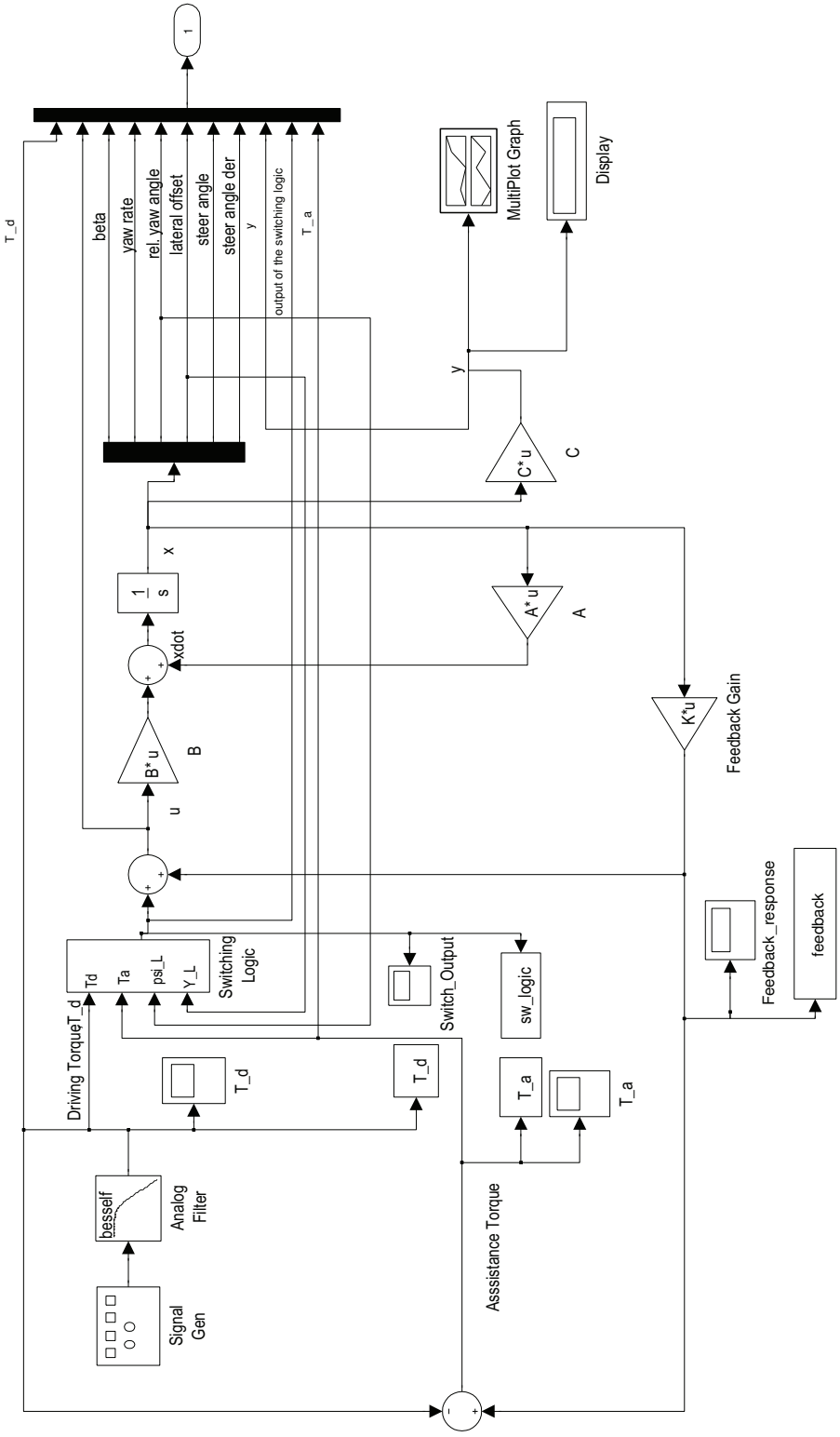

Fig. A.1. LIVIC controller model.

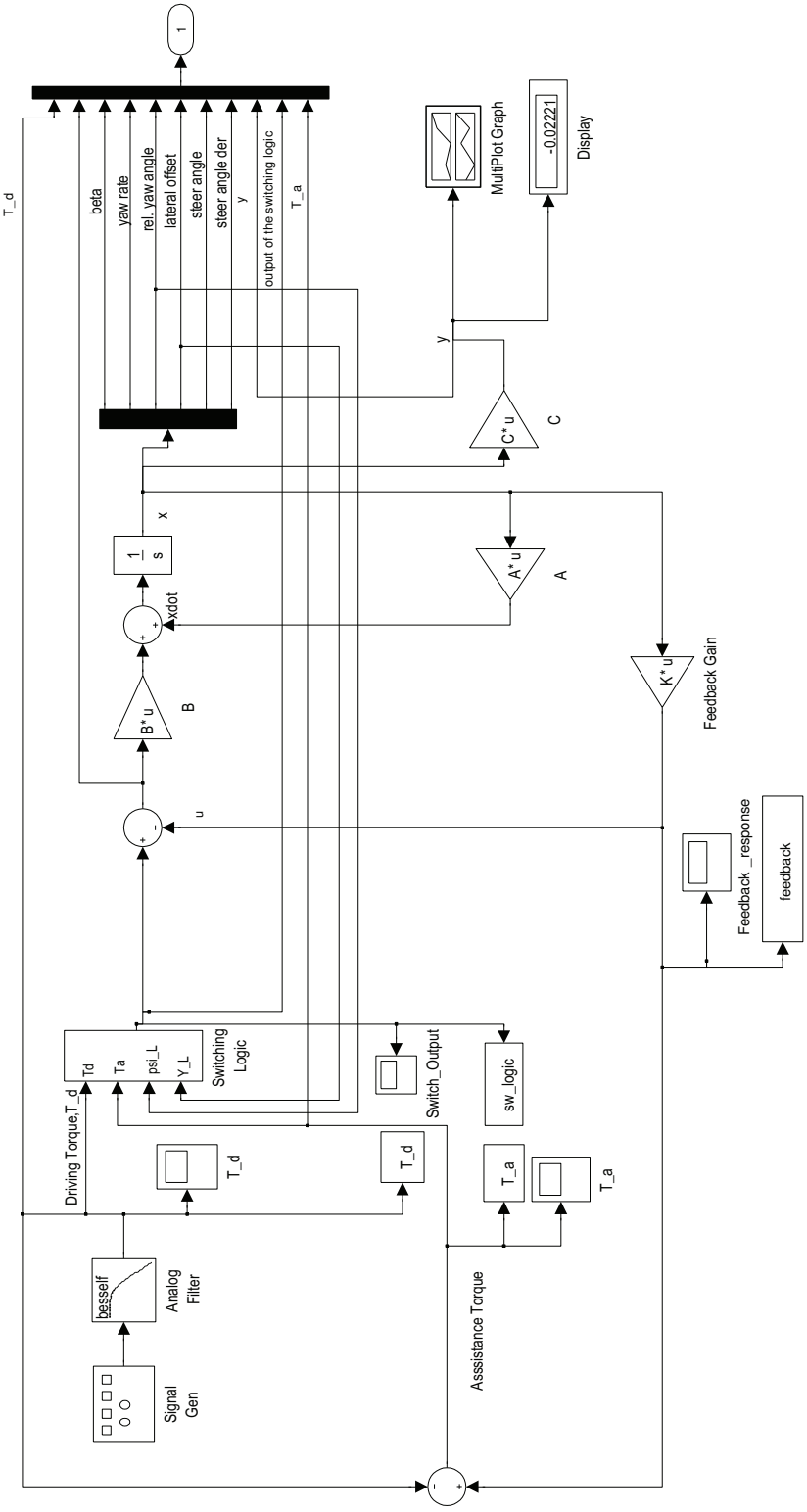

Fig. A.2. New controller model.

Appendix B: Matlab Scripts

In this chapter, we have presented the script used to model the LQR controller for the new switching strategy (LQR script).

```
A = [-6.2500 -0.9911 0 0  3.3333 0;
      1.3040 -7.1780 0 0 39.7718 0;
      0 1 0 0 0 0;
      15 0.98 15 0 0 0;
      0 0 0 0 0 1;
      812.5 66.0833 0 0 -812.5 -300]
B = [0;0;0;0;0;1.2500]
disp('Controllability Matrix:')
contro_1 = [B A*B A^2*B A^3*B A^4*B A^5*B]
disp('Rank of Controllability Matrix')
rank(contro_1)
C = [0 1 0 1 1 0]
disp('Observability Matrix:')
observablity = [C;C*A;C*(A^2);C*(A^3);C*(A^4);C*(A^5)]
disp('Rank of Observability Matrix')
rank(observablity)

%%% Design LQR filter with diagonal state weighting matrix
%%% and unit input weighting matrix

Q = [20 0 0 0 0 0;
     0 4 0 0 0 0;
     0 0 1 0 0 0;
     0 0 0 1000 0 0;
     0 0 0 0 20 0;
```

```
     0 0 0 0 0 100]

[K,s,e] = lqr(A,B,Q,1,0)

Ad=(A-B*K)

eig(Ad)

sys = ss(Ad,B,C,0)

[Stable,PhaseMargin] = loopmargin(sys)

%unit-step response
figure(1)
t=0:0.01:30;
y = step(Ad,B,C,0,1,t);
plot(t,y)
grid
title('Unit-Step Response')
xlabel('sec')
ylabel('output')

%lyapnov stability
P=lyap(Ad,Q)

%root-locus
figure(2)
rlocus(sys)
sgrid
```

```
%%% Run simulation of controlled system.

[t,x,y] = sim('Controller_code1026');
figure(3)

  plot(t,y(:,1))
xlabel('Time (sec)')
ylabel('Driving Torque (Nm)')
%legend('Tau','u','x','y')
grid
figure(4)
  plot(t,y(:,3))
xlabel('Time')
ylabel('Slip Angle')
grid
figure(5)
 plot(t,y(:,4))
xlabel('Time')
ylabel('Yaw Rate')
grid
figure(6)
plot(t,y(:,5))
xlabel('Time')
ylabel('Yaw Angle')
grid
figure(17)
  plot(t,y(:,6))
xlabel('Time')
```

```
ylabel('Lateral Offset')
grid
figure(18)
plot(t,y(:,7))
xlabel('Time')
ylabel('Steering Angle')
grid
figure(19)
plot(t,y(:,8))
xlabel('Time')
ylabel('Steering Angle Derivative')
grid

figure(7)
[AX,H1,H2] = plotyy(t,y(:,3),t,y(:,6),'plot')
xlabel('Time (sec)');
set(get(AX(1),'Ylabel'),'String','Angle (rad)')
set(get(AX(2),'Ylabel'),'String','Distance (m)')
set(H1,'LineStyle','--')
set(H2,'LineStyle','-.')
% plot(t,y(:,3),'-',t,y(:,6),'-.')
legend('Slip Angle','Lateral Offset')
% xlabel('Time')
grid

figure(8)
plot(t,y(:,4),'-',t,y(:,8),'-.')
legend('Yaw Rate','Steering Angle Rate')
xlabel('Time (sec)')
```

```
ylabel('Angle (rad/sec)')
grid

figure (36)
[AX,H1,H2] = plotyy(t,y(:,5),t,y(:,6),'plot')
xlabel('Time (sec)');
set(get(AX(1),'Ylabel'),'String','Angle (rad)')
set(get(AX(2),'Ylabel'),'String','Distance (m)')
set(H1,'LineStyle','--')
set(H2,'LineStyle','-.')
% plot(t,y(:,3),'-',t,y(:,6),'-.')
legend('Yaw Angle','Lateral Offset')
grid

figure(9)
plot(t,y(:,5),'-',t,y(:,7),'-.')
legend('Yaw Angle','Steering Angle')
xlabel('Time (sec)')
ylabel('Angle (rad)')
grid

figure(10)
%Trajectory of the front wheels
y_l=(y(:,6)+(1.22-0.95)*y(:,5))+(1.5/2);
y_r=(y(:,6)+(1.22-0.95)*y(:,5))-(1.5/2);
plot(t,y_l,'-',t,y_r,'-.')
legend('y_l','y_r')
xlabel('Time (sec)')
ylabel('Trajectory of the front wheels')
```

```
grid

figure(12)
plot(t,T_d,'-',t,T_a,':',t,sw_logic,'-.',t,states,'--')
legend('T_d','T_a','Output of the switching logic',
'Response of y_L + 0.27psi_L')
xlabel('Time (sec)')
ylabel('switching curve (Torque (Nm))')
grid

figure(13)
plot(t,y(:,11),':',t,y(:,1),'--')
legend('Assistance Torque T_a','Driving Torque T_d')
ylabel ('Torque (Nm)')
xlabel('Time (sec)')
grid
```

Appendix C: Matlab Results

This chapter documents the results for the LQR script used to design the controller.

```
A =

   -6.2500   -0.9911         0         0    3.3333         0
    1.3040   -7.1780         0         0   39.7718         0
         0    1.0000         0         0         0         0
   15.0000    0.9800   15.0000         0         0         0
         0         0         0         0         0    1.0000
  812.5000   66.0833         0         0 -812.5000 -300.0000


B =

         0
         0
         0
         0
         0
    1.2500

Controllability Matrix:
contro_1 =

  1.0e+012 *

         0         0    0.0000   -0.0000    0.0000   -0.0001
         0         0    0.0000   -0.0000    0.0000   -0.0013
```

```
         0         0         0    0.0000   -0.0000    0.0000
         0         0         0    0.0000   -0.0000    0.0000
         0    0.0000   -0.0000    0.0000   -0.0000    0.0098
    0.0000   -0.0000    0.0000   -0.0000    0.0098   -2.9267

Rank of Controllability Matrix
ans =

     6
C =

     0     1     0     1     1     0

Observability Matrix:
observablity =
  1.0e+010 *

         0    0.0000         0    0.0000    0.0000         0
    0.0000   -0.0000    0.0000         0    0.0000    0.0000
    0.0000    0.0000         0         0   -0.0000   -0.0000
   -0.0000   -0.0000         0         0    0.0000    0.0000
    0.0064    0.0005         0         0   -0.0064   -0.0023
   -1.9000   -0.1616         0         0    1.9037    0.6806

Rank of Observability Matrix
ans =

     6
Q =
```

```
    20     0     0     0     0     0
     0     4     0     0     0     0
     0     0     1     0     0     0
     0     0     0  1000     0     0
     0     0     0     0    20     0
     0     0     0     0     0   100

K =

  315.9293   44.0141  489.7011   31.6228  682.5164    2.4707

s =
  1.0e+005 *

    0.3629    0.0512    0.5753    0.0431    0.7615    0.0025
    0.0512    0.0079    0.0869    0.0070    0.1063    0.0004
    0.5753    0.0869    0.9678    0.0799    1.1836    0.0039
    0.0431    0.0070    0.0799    0.0103    0.0767    0.0003
    0.7615    0.1063    1.1836    0.0767    1.6485    0.0055
    0.0025    0.0004    0.0039    0.0003    0.0055    0.0000

e =
  1.0e+002 *

  -2.9747
  -0.1138
  -0.0248 + 0.0181i
  -0.0248 - 0.0181i
```

```
  -0.0135 + 0.0169i
  -0.0135 - 0.0169i

Ad =
  1.0e+003 *

   -0.0063   -0.0010         0         0    0.0033         0
    0.0013   -0.0072         0         0    0.0398         0
         0    0.0010         0         0         0         0
    0.0150    0.0010    0.0150         0         0         0
         0         0         0         0         0    0.0010
    0.4176    0.0111   -0.6121   -0.0395   -1.6656   -0.3031

ans =
  1.0e+002 *

  -2.9747
  -0.1138
  -0.0248 + 0.0181i
  -0.0248 - 0.0181i
  -0.0135 + 0.0169i
  -0.0135 - 0.0169i

a =
            x1       x2       x3       x4       x5       x6
   x1    -6.25  -0.9911        0        0    3.333        0
   x2    1.304   -7.178        0        0    39.77        0
   x3        0        1        0        0        0        0
   x4       15     0.98       15        0        0        0
```

```
   x5        0        0        0        0        0        1
   x6    417.6    11.07   -612.1   -39.53    -1666   -303.1

b =
         u1
   x1     0
   x2     0
   x3     0
   x4     0
   x5     0
   x6  1.25

c =
       x1  x2  x3  x4  x5  x6
   y1   0   1   0   1   1   0

d =
       u1
   y1   0

Continuous-time model.

Stable =
     GainMargin: Inf
    GMFrequency: Inf
    PhaseMargin: [1x0 double]
    PMFrequency: [1x0 double]
    DelayMargin: [1x0 double]
    DMFrequency: [1x0 double]
```

```
         Stable: 1

PhaseMargin =
    PhaseMargin: [-88.9218 88.9218]
      Frequency: 1.8480

P =
  1.0e+003 *

    0.0019   -0.0013   -0.0011    0.0117    0.0002    0.0023
   -0.0013    0.0704   -0.0005   -0.1719    0.0127   -0.0458
   -0.0011   -0.0005    0.0126   -0.0338   -0.0018   -0.0127
    0.0117   -0.1719   -0.0338    1.8676   -0.0325    0.0122
    0.0002    0.0127   -0.0018   -0.0325    0.0034   -0.0100
    0.0023   -0.0458   -0.0127    0.0122   -0.0100    0.0806
```